energy&fuels

Article

pubs.acs.org/EF

In Situ and ex Situ Catalytic Pyrolysis of Pine in a Bench-Scale Fluidized Bed Reactor System

Kristiina Iisa,*[,†] Richard J. French,[†] Kellene A. Orton,[†] Matthew M. Yung,[†] David K. Johnson,[†] Jeroen ten Dam,[‡] Michael J. Watson,[‡] and Mark R. Nimlos[†]

[†]National Renewable Energy Laboratory, Golden, Colorado 80401, United States

[‡]Johnson Matthey Technology Centre, Billingham, Cleveland, TS23 1LB, U.K.

Supporting Information

ABSTRACT: In situ and ex situ catalytic pyrolysis were compared in a system with two 2-in. bubbling fluidized bed reactors. Pine was pyrolyzed in the system with a catalyst, HZSM-5 with a silica-to-alumina ratio of 30, placed either in the first (pyrolysis) reactor or the second (upgrading) reactor. Both the pyrolysis and upgrading temperatures were 500 °C, and the weight hourly space velocity was 1.1 h^{-1}. Five catalytic cycles were completed in each experiment. The catalytic cycles were continued until oxygenates in the vapors became dominant. The catalyst was then oxidized, after which a new catalytic cycle was begun. The in situ configuration gave slightly higher oil yield but also higher oxygen content than the ex situ configuration, which indicates that the catalyst deactivated faster in the in situ configuration than the ex situ configuration. Analysis of the spent catalysts confirmed higher accumulation of metals in the in situ experiment. In all experiments, the organic oil mass yields varied between 14 and 17% and the carbon efficiencies between 20 and 25%. The organic oxygen concentrations in the oils were 16−18%, which represented a 45% reduction compared to corresponding noncatalytic pyrolysis oils prepared in the same fluidized bed reactor system. GC/MS analysis showed the oils to contain one- to four-ring aromatic hydrocarbons and a variety of oxygenates (phenols, furans, benzofurans, methoxyphenols, naphthalenols, indenols). High fractions of oxygen were rejected as water, CO, and CO_2, which indicates the importance of dehydration, decarbonylation, and decarboxylation reactions. Light gases were the major sources of carbon losses, followed by char and coke.

1. INTRODUCTION

Catalytic fast pyrolysis is a promising method for producing liquid transportation fuels or biofuels. Biomass can be converted to a liquid product by fast pyrolysis in high yields, but the product oil is unsuitable as a biofuel due to properties imparted by its high oxygen content, including low heating value, high acidity, high distillation residue, immiscibility with petroleum products, and reactions during storage.[1,2] In catalytic fast pyrolysis, vapors from biomass pyrolysis are contacted with a catalyst at atmospheric pressure to upgrade vapors prior to their condensation. Zeolites, in particular HZM-5, have been efficient in deoxygenating the vapors by a combination of dehydration, cracking, isomerization, cyclization, and aromatization reactions.[3−9]

The upgrading catalyst may be placed in the pyrolysis reactor (in situ catalytic fast pyrolysis) or in a separate reactor through which pyrolysis vapors are passed prior to condensation (ex situ catalytic fast pyrolysis or vapor-phase upgrading). A design report detailing both in situ and ex situ catalytic pyrolysis was published recently.[10] The advantages of in situ catalytic pyrolysis include lower capital cost due to a simpler process configuration (one reactor). The advantages of ex situ catalytic pyrolysis include the ability to optimize pyrolysis and catalytic upgrading separately and separating the catalyst from the contaminants in the biomass.[10,11]

Catalytic pyrolysis has been studied in both in situ and ex situ configurations. Early work concentrated on ex situ upgrading of pyrolysis vapors[12−17] or vaporized pyrolysis oils.[3,18,19] Investigations have been conducted in several different bench-scale reactor configurations, for example, bubbling fluidized beds in the in situ configuration[6,20−29] and ex situ configuration.[30−33] Other experimental systems include in situ conical spouted beds,[34,35] in situ fixed beds with constant catalysts feed,[36−39] in situ circulating fluidized bed,[40,41] and ex situ fixed beds.[3,5,12−18,42] Catalyst and parameter screening studies have been also extensively performed in microscale analytical pyrolysis units (Py−GC/MS).[8,43−47]

Promising results have been obtained in both configurations, but there are few direct comparisons of in situ and ex situ catalytic pyrolysis in industrially relevant reactors. Yildiz et al.[48] compared in situ and ex situ catalytic pyrolysis over HZSM-5 in a system with an auger pyrolysis reactor using catalyst (in situ) or sand (ex situ) as the heat-transfer medium and catalyst in a separate moving bed reactor for ex situ experiments. In general, better performance was found in the in situ experiments: liquid carbon yields and aromatic yields were higher. The ex situ configuration produced more solids, while the in situ configuration produced more CO. A correlation between CO yields and aromatics yields was found, whereas CO_2 yields were similar to those for noncatalytic pyrolysis, suggesting that the catalyst increased decarbonylation reactions but had little impact on decarboxylation reactions.

Gungor et al.[49] compared the two configurations in a bench-scale fixed bed system for slow pyrolysis (7 °C/min) of pine bark using ReUS-Y zeolite, and Nguyen et al.[50] did the same in fixed

Received: September 23, 2015
Revised: February 2, 2016

DOI: 10.1021/acs.energyfuels.5b02165
Energy Fuels XXXX, XXX, XXX−XXX

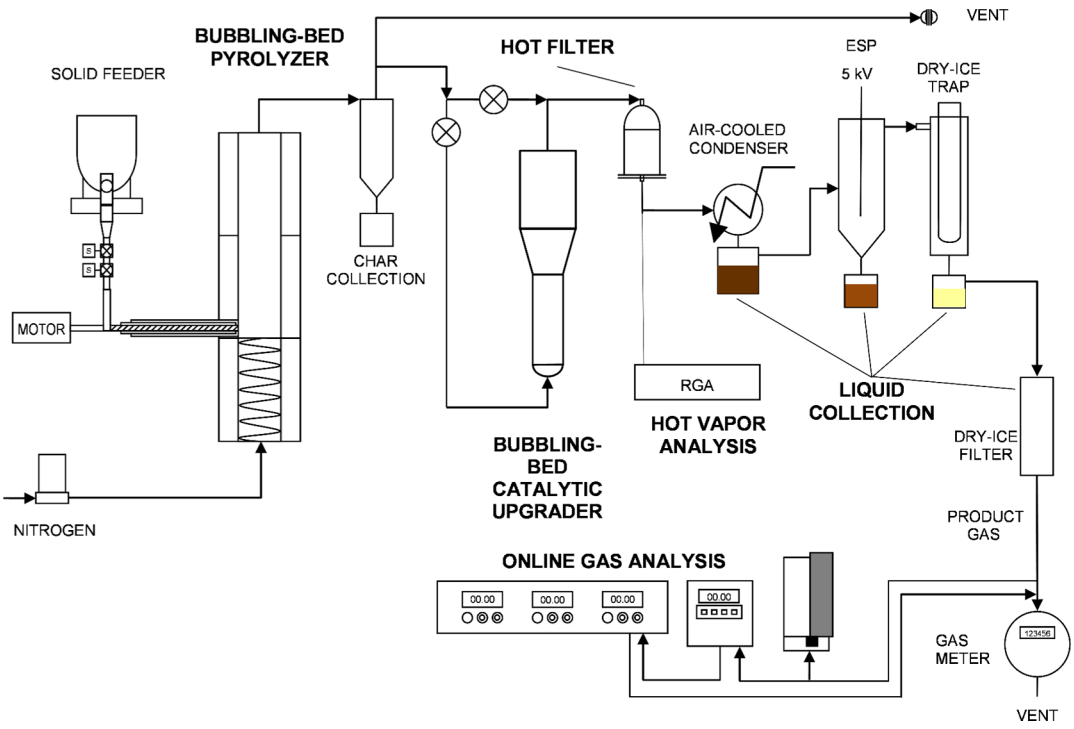

Figure 1. Schematic of the 2" fluidized bed reactor system. In in situ experiments, the catalyst was placed in the pyrolyzer and the catalytic upgrader was bypassed. In ex situ experiments, sand was used as the fluidizing media and the catalyst was in the catalytic upgrader.

bed reactors with faster heating rates (heating to 500 °C in 10 s) for pine over faujasite ($Na_{0.2}H_{0.8}FAU$). Both found some deoxygenation in the ex situ confirmation but not in the in situ configuration.

In situ and ex situ catalytic pyrolysis over HZSM-5 have also been compared in microscale analytical pyrolysis (Py−GC/MS) by Wang et al.,[51] Gamliel et al.,[52] and Wan and Wang.[11] In situ catalytic pyrolysis was found to give higher aromatics yields than ex situ catalytic pyrolysis, in particular at high mass ratios of catalyst to biomass, when the catalyst is active.[11,51,52] Ex situ catalytic pyrolysis favored monocyclic aromatics, while the in situ method favored naphthalenes and higher aromatics.[51,52] Wan and Wang[11] found less complete deoxygenation in ex situ experiments, whereas Gamliel et al.[52] reported higher oxygenates for in situ experiments. No oxygenates were detected by Wang et al.[51] due to the high catalyst-to-biomass ratio in that study. Wang et al.[51] reported higher olefin yields for ex situ catalytic pyrolysis, and Gamliel et al.[52] found higher gas yields.

Gamliel et al.[52] further compared the results from their Py−GC/MS experiments to those from in situ catalytic pyrolysis in a spouted bed reactor in a previous study.[35] The composition of oil from the in situ spouted bed experiment resembled that from the ex situ Py−GC/MS experiment and not that from the in situ Py−GC/MS vapor. There are several possible explanations for the lack of the correspondence between the in situ catalytic pyrolysis vapors from Py−GC/MS and the in situ oil from the spouted bed reactor. I situ fixed bed systems with a batch of catalyst and biomass that need to be heated simultaneously suffer from an incongruity between biomass pyrolysis temperature and catalyst activity. Some compounds evolve at low temperatures, when the catalyst is not active. This can explain the low deoxygenation for in situ measurements in several of the comparisons. Other potential problems for these types of in situ experiments include poor solid/solid contact and heat transfer.[11,50,51] Differences in pyrolysis vapor concentrations and vapor residence times also contribute to difficulties in some of the comparisons of ex situ and in situ catalytic pyrolysis.[11]

Aho et al.[53] reviewed results of their previous studies made in a single fluidized bed system (in situ) and a dual fluidized bed system (ex situ). The dual-bed configuration was adopted as a more reliable method to study catalytic pyrolysis, and several improvements in the system were made, including faster heating in the pyrolysis zone, improved condensation system, and addition of gas analysis capabilities. Consequently, the results could not be used to study the differences between in situ and ex situ catalytic pyrolysis.

The objective of the current work was to compare in situ and ex situ catalytic pyrolysis performed in similar reactors with constant catalyst temperature and fast heating of the biomass. The use of fluidized bed reactors for the comparison eliminated many of the difficulties associated in other comparisons of the two configurations. While there are numerous studies of catalytic pyrolysis in both configurations, to the authors' knowledge, there are no direct comparisons under identical conditions in fluidized bed reactors. In the current contribution, pine vapors were upgraded over HZSM-5 catalysts placed either in a bubbling fluidized bed pyrolyzer or upgrading reactor. The two reactors had the same diameters and the same weight hourly space velocities, the catalysts were preheated to the reaction temperature in both configurations, and the pyrolysis fluidized bed provided rapid heating of the biomass powder. The impact of the reactor configuration—in situ or ex situ—on oil yields, oil quality, and catalyst deactivation was assessed.

2. EXPERIMENTAL SECTION

2.1. Fluidized Bed Reactor System. Catalytic pyrolysis tests were performed using a 2-in. fluidized bed reactor system, as shown in Figure 1. The first reactor (pyrolyzer) had an inner diameter (i.d.) of 5.2 cm and comprised a coiled tube preheater, a dual perforated-plate distributor, and a 43 cm tall straight-walled stainless steel reaction/disengagement

DOI: 10.1021/acs.energyfuels.5b02165
Energy Fuels XXXX, XXX, XXX−XXX

Table 1. Composition of Pine

	C	H	N	S	O (direct)[a]	moisture	ash
wt %	49.6	6.3	0.05	0.12	43.5	2.9	0.33
	Al	Ca	Cr	Cu	Fe	K	Mg
μg/g	<1	968 ± 5	<3	<2	2.8 ± 0.2	477 ± 2	225 ± 3
	Mn	Na	Ni	P	S	Zn	
μg/g	89 ± 1	24 ± 1	<3	58 ± 2	82 ± 2	<0.2	

[a]By ASTM D5622.

section. The second reactor (upgrader) comprised a dual perforated plate followed by a 15 cm tall, 5.2 cm diameter i.d. reaction zone and a 7.8 cm diameter disengagement section. In in situ experiments, the catalyst was placed in the pyrolyzer and the catalytic upgrader was bypassed. In ex situ experiments, sand was used as the fluidizing media and the catalyst was in the catalytic upgrader. The reactors were both operated at a temperature of 500 °C.

Nitrogen (14 sL/min) at a pressure slightly above atmospheric was used as a fluidizing gas. Pine wood of particle size less than 0.5 mm was augered into the pyrolyzer at a rate of 150 g/h controlled by a K-Tron loss-in-weight feeder. Char and fine bed material were removed in a cyclone immediately following the pyrolyzer and a 2 μm stainless steel mesh hot-gas filter immediately before the condensation train. The vapors were cooled and condensed in an air-cooled condenser (exit gas temperature approximately 60 °C) with an ice-cooled receiver, an electrostatic precipitator, a dry ice trap, and a dry ice cooled coalescing filter kept at 0 °C on the filter surface. All parts between the pyrolyzer and condenser were kept at 400−500 °C via electric heat tracing. The process gas flow rate was monitored by a mass flow meter and measured by a dry test meter. Vapor species were monitored by a residual gas analyzer (RGA) (Dycor Dymaxion by Ametek). The concentrations of CO_2, CO, and methane in the product gas were monitored by a nondispersive infrared analyzer (NDIR model 300 from California Analytical Instruments). In addition, the gas was analyzed every 4 min by an online Varian micro gas chromatograph equipped with molecular sieve 5A, Porabond Q, and CP-Sil columns for analysis of hydrogen, carbon monoxide, carbon dioxide, methane, C_2−C_4 hydrocarbons, and nitrogen. The temperatures in the system, as well as the flows, were recorded and controlled by the OPTO 22 data acquisition and control system.

2.2. Materials. The feed was Southern yellow pine, provided by Idaho National Laboratory, and was ground to a particle size of less than 0.5 mm. The ultimate analysis and the contents of selected elements measured by ICP are given in Table 1. Two HZSM-5 catalysts, both with a silica-to-alumina ratio (SAR) of 30, were tested. SAR 30 was selected because it has been found to give the highest aromatic yields.[54,55] Catalyst A was provided by Nexceris and had clay (bentonite, 12 wt %) as binder. The particle size was 500−1000 μm. Catalyst B was provided by Johnson Matthey and it was prepared using ZSM-5 and a silica-based binder to give a catalyst with an approximate composition of 20% SiO_2 binder and 80% ZSM-5. The sodium content of catalyst B was determined to be 0.24 wt %. The sodium in the catalyst arises from the use of the silica binder; the parent ZSM-5 had a sodium content below 0.01%. The particle size range was 300−1000 μm. Catalyst B was precalcined by the manufacturer and was used as received. Catalyst A was calcined according to the manufacturer's instructions by holding it at 500 °C for 4 h in a flow of nitrogen in the reactor prior to beginning the experiment. Both catalysts were initially tested for in situ catalytic pyrolysis, and the better performing one was selected for the in situ vs ex situ comparison.

2.3. Procedure. The charge to either fluidized bed was 200 mL of solids. The reactors were heated to 500 °C under flowing nitrogen. When the operating temperature was reached, the condensation train was cooled and connected in line with the reactor. Feeding commenced and the composition of the vapors was monitored with the RGA. A gas-bag sample of the cooled product gas was collected near the start and end of the catalytic pyrolysis time.

The RGA signals for selected aromatics and oxygenates were monitored during the experiment. The catalytic pyrolysis cycle was continued until the catalyst was deemed deactivated according to the RGA data; i.e., when the aromatics signals had decreased to approximately 10% of the initial value, the highest oxygenate signal became comparable to the highest hydrocarbon signal, and the signal for acetic acid (m/z = 60) began to increase rapidly. Then the biomass feeding was stopped, the condenser was bypassed, and the catalyst was regenerated by applying 0.2−3.2 sL/min air and enough nitrogen to keep the air concentration less than 50%. When the carbon dioxide (CO_2) level fell below approximately 0.1%, the catalyst was considered regenerated and a new cycle of pyrolysis was begun.

Five catalytic cycles were completed in each experiment. The catalyst from the final cycle was recovered without regeneration. Parameters for the three experiments performed are listed in Table 2. In situ catalytic pyrolysis was performed with both catalysts but ex situ catalytic pyrolysis only with catalyst B. The weight hourly space velocity was 1.1 g/(g h) in all experiments.

Table 2. Experimental Parameters for the Catalytic Pyrolysis Runs

experiment	pyrolyzer	upgrader	catalyst (g)	cycles	biomass fed (g)
cat. A in situ	catalyst A	bypassed	131	5	786
cat. B in situ	catalyst B	bypassed	139	5	1056
cat. B ex situ	silica sand	catalyst B	139	5	1223

The total liquid yields in the experiments were determined from the mass increase in the collection system, including the oil collection vessels, the condensers, ESP, coalescing filter, and the filter housing. The amount of coke formed in cycles 1−4 was calculated from the CO and CO_2 released during the oxidation of the catalyst beds after each cycle, and for the last cycle (cycle 5) it was based on the initial mass of catalyst and analysis of coked catalyst after the experiment. The char yield was determined as the difference in the total solid mass gain in the system and coke from the last cycle. The total solids mass included the mass increase in the pyrolyzer bed and upgrader bed materials and the mass increase in the cyclone and hot gas filter. Duplicate catalytic pyrolysis experiments in the same reactor system have shown yields (oil, aqueous, gas, coke) to be within one percentage point of each other.[56]

2.4. Analyses. The liquids (top and bottom organic fraction, aqueous fraction) and solids (feed, char, and catalyst before and after experiments) were analyzed for C, H, and N contents by a modified ASTM D5373 method, for S by ASTM D4239, and for ash residue by modified ASTM D3174 (micro size). The water content in the liquids was determined by Karl Fisher titration according to ASTM E1064 and direct oxygen according to ASTM D5622. All of these analyses were performed by Huffman Laboratories, Inc., Golden, CO.

Carboxylic acid contents were determined for the liquid fractions by potentiometric titration of samples dissolved in ethanol.[57] Titrant was standardized NaOH in water. This method identifies only carboxylic acids, and a carboxylic acid number (CAN) was determined from the titration. Carbonyl (ketones and aldehydes) contents were quantified by oxime titration.[57] The aging behavior of the oils was determined by measuring the viscosity before and after holding the oils at 90 °C for 18 h. The viscosity was measured by a Brookfield DVT2T viscometer in triplicate.

DOI: 10.1021/acs.energyfuels.5b02165
Energy Fuels XXXX, XXX, XXX−XXX

The liquid samples were analyzed for chemical composition by an Agilent 6890 GC equipped with a 5973 MS (Agilent Technologies, Palo Alto, CA). Sample compounds were separated using a 30 m × 0.25 mm × 0.25 μm HP-5MS column (Agilent 122-5532). HP MSD Chemstation software (Agilent) equipped with NIST database Rev. D.03.00 was used to determine the identity of the unknown compounds found within the samples. Prior to analysis, the samples were diluted in acetone in an oil:acetone ratio of 1:40 for the bottom organic liquids and in the ratio 1:10 for the other liquids. Each sample was placed on an autosampler (Agilent) and injected at a volume of 1 μL into the GC/MS (Agilent). The GC/MS method consisted of a front inlet temperature of 285 °C, MS transfer line temperature of 280 °C, and a scan range from 35 to 450 m/z. A constant flow of 1 mL/min was held throughout the run. A starting temperature of 35 °C was held for 3 min, ramped at 15 °C/min to a temperature of 225 °C, held for 1 min, continued at a ramped rate of 15 °C/min to 300 °C, and held for 5 min. The method resulted in a run time of 26.7 min for each sample.

The liquid fractions were also analyzed by ^{13}C NMR. A 0.5 g portion of the liquids was dissolved in $CDCl_3$. Spectra were collected on a Bruker Avance 600 sepctrometer at 150.92 MHz, with inverse gated coupling, recycle delay of 10 s, 90° pulse for 10 μs, and 4096 averaged scans (11 h 50 min total time). The assignments were made according to the work of Ben and Ragauskas;[58] however, no distinction between aromatic C−H and C−C was made due to the large overlap in this region. The assignments were bs follows: C═O, 215.0−166.5 ppm; aromatic C−O, 166.5−142.0 ppm; aromatic C−C and C−H, 142.0−95.8 ppm; aliphatic C−O, 95.8−60.8 ppm; methoxyl, 60.6−60.8 ppm; and aliphatic C−C, 60.8−0 ppm.

The molecular weight distribution in the organic oil fractions was determined by gel permeation chromatography (GPC). The 50 mg samples were dissolved in 50 mL of tetrahydrofuran (THF, Baker HPLC grade). The dissolved samples were filtered (0.45 μm nylon membrane syringe filters) before GPC analysis. GPC analysis was performed using an Agilent HPLC with three GPC columns (Polymer Laboratories, 300 × 7.5 mm) packed with polystyrene-divinylbenzene copolymer gel (10 μm beads) having nominal pore diameters of 10^4, 10^3, and 10^2 Å, respectively. The eluent was THF and the flow rate 1.0 mL/min. The sample concentration was 1− 2 mg/mL and an injection volume of 25 μL was used. The HPLC was attached to a diode-array detector measuring absorbance at 260 nm (bandwidth 40 nm). Retention time was converted into molecular weight by applying a calibration curve established using 18 polystyrene standards of known molecular weight [range from 1 × 10^6 to 580 Da plus toluene (92)]. The molecular weights calculated are not absolute molecular weights but are an approximation based on the polystyrene calibration standards.

The gas-bag samples were analyzed for light organics (condensables) on an Agilent Technologies 7890A GC system equipped with a FID and an Agilent Technologies 5975C inert XL mass selective detector (MSD). The GC system was fitted with an Agilent 19091S-433 HP-5MS capillary GC column with a length of 30 m, 0.250 mm i.d., and a 0.25 μm film thickness (5% phenyl−95% methylsiloxane). The oven temperature was held at 30 °C for 5 min before ramping at 10 °C/min to 270 °C. The MSD signal was used for compound identification and the FID signal for quantification. Semiquantitative analysis was done by measuring the FID response factor for cyclohexanol and applying the response factor to the compounds with adjustments for the molecular structure.[59] The water vapor content in the exit gases was estimated by assuming that the gas was saturated at the temperature of the coalescing filter (0 °C).

2.5. Catalyst Characterization. Fresh catalysts, spent (coked) catalysts, and the corresponding regenerated catalysts were analyzed by a variety of methods. For catalyst A, the fresh sample for catalyst characterization was prepared by calcining for 4 h at 500 °C in N_2. Catalyst B was already calcined by the manufacturer, and no additional calcining was performed prior to the characterization. The regenerated catalysts were prepared for analysis by heating for 4 h at 550 °C in a mixture of N_2 and air (50:50).

In order to quantify the number of acid sites on the catalyst materials, temperature-programmed ammonia desorption (NH_3 TPD) was conducted. Catalyst samples (200 mg) were loaded in a quartz U-tube and evaluated on a microflow reactor system (AMI-390) equipped with a thermal conductivity detector. Fresh catalysts were pretreated by heating in 10% O_2/Ar to 500 °C, holding for 60 min, and then cooling to 120 °C in He flow, following which the adsorption step was performed. This consisted of flowing 10% NH_3/He for 30 min at 120 °C, followed by flushing with He. The TPD was performed by heating at 30 °C/min from 120 to 500 °C, with a 30 min hold at 500 °C. The gas flow rate in all steps was 25 sccm. A sample loop of known volume was used to calibrate the thermal conductivity detector (TCD) response for NH_3 and quantify the amount of NH_3 desorbed from the samples. For coked catalysts, the number of acid sites was determined as described above, except the initial heating step was performed in an inert gas (He); the catalyst was then regenerated by flowing 10% O_2/Ar over the catalysts at 550 °C for 30 min, after which a second TPD was performed.

The HZSM-5 phases were confirmed using XRD on a Bruker D8 spectrometer. The spectra were recorded with a Cu $K\alpha$ emission wavelength of 1.5406 Å at 0.02 2θ/s.

The amount of coke on the catalyst at the end of an experiment was measured by thermogravimetric analysis (TGA) in a TGA Setaram (TN688, SETSYS Evolution) analyzer. The spent catalysts were heated in air at 20 °C/min from 25 to 780 °C. The mass loss from approximately 250 to 650 °C was attributed to coke while that below 250 °C was associated with water and weakly adsorbed organic species. A control test was performed with fresh catalyst to ascertain that there was no mass loss in the fresh catalyst in the coke region. This gave the coke remaining after the fifth cycle. For the other cycles, the amount of carbon in coke was determined from the CO_2 and CO concentrations during regeneration measured by the NDIR analyzers and the gas flow rates. This was converted to mass of coke by the elemental composition of coke determined by the ultimate analysis of the spent catalysts from the last cycle.

The fresh, spent, and regenerated samples were analyzed by a Spectro-Arcos SOP radial view inductively coupled plasma atomic emission spectrograph (ICP-AES) for Al, Ca, Cr, Cu, Fe, K, Mg, Mn, Na, Ni, P, S, Zn contents. The samples were weighed out (~500 mg) in triplicate. Five milliliters of 72 wt % nitric acid (reagent grade) was added to each sample; they were heated to 150 °C over 10 min and then held at 150 °C for 10 min before cooling to room temperature. The samples were each filtered through a glass-fiber filter and diluted to a final volume of 25 mL with deionized water. The ICP-AES was equipped with an argon-purged optical path to allow analysis of elemental emission lines in the range of 130−773 nm. All lines were acquired at 1425 W plasma power. The ICP-AES was calibrated using commercial 1000 ppm standards diluted with nitric acid solution (1 volume concd nitric acid + 4 volumes deionized water).

The activities of fresh, spent, and regenerated catalysts for upgrading pyrolysis vapors were determined by analytical pyrolysis in a pyroprobe (model 5200HP-R, CDS Analytical Inc.) coupled to an Agilent G1530A gas chromatograph (GC) interfaced with a HP 5973 mass spectrometer (MS). Approximately 1 mg of biomass topped by 10 mg of catalyst was placed in a sample tube inside a computer-controlled resistively heated element and pyrolyzed at 500 °C. Products from the pyrolysis zone were entrained in He carrier gas and flowed through a trap filled with Tenax-TA (a polymer resin, poly(2,6 diphenyl-*p*-phenylene oxide). Light gases passed through the trap but most of the vapors were adsorbed onto it. After 3 min, the trap was heated to 400 °C to desorb the adsorbed vapors and the He carrier gas (52 mL/min) passed the vapors to the GC. The trap was heated to 400 °C. The transfer lines from the trap to the GC were heated to 325 °C, the interface was held at 70 °C, and the GC injector was operated at 275 °C. The vapors were separated in an Agilent 190915-433 capillary column with a stationary phase consisting of 5% phenyl and 95% dimethylpolysiloxane. The GC oven was programmed with a hold of 3 min at 40 °C followed by heating to 240 °C at 6.0 °C/min. The separated species were identified using the NIST GC/MS library. The GC/MS was calibrated for 42 compounds consisting of hydrocarbons and oxygenates typically detected in upgraded biomass pyrolysis vapors (see Table 1 in Supporting Information). Response factors for noncalibrated compounds were selected on the basis of similar compounds. The carbon yields of organic vapors were calculated by adding up the carbon detected in each compound and dividing by carbon in the biomass.

DOI: 10.1021/acs.energyfuels.5b02165
Energy Fuels XXXX, XXX, XXX−XXX

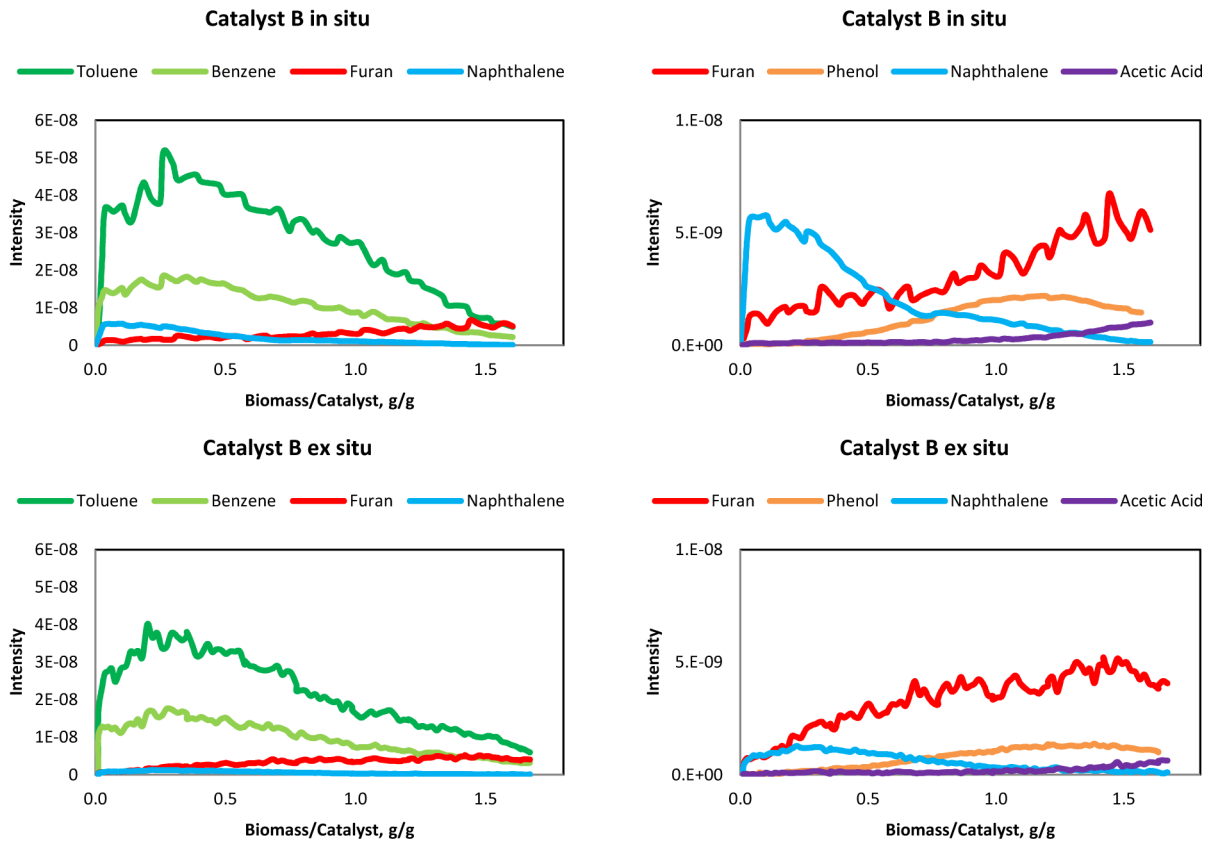

Figure 2. RGA signals for selected compounds during cycle 2 for in situ and ex situ catalytic pyrolysis with catalyst B. The m/z values used for the compounds were toluene, 91; benzene, 78; naphthalene, 128; furan, 68; phenol, 96; acetic acid and hydroxyacetaldehyde, 60. A biomass:catalyst ratio of 1 corresponds to 55 min of time on stream.

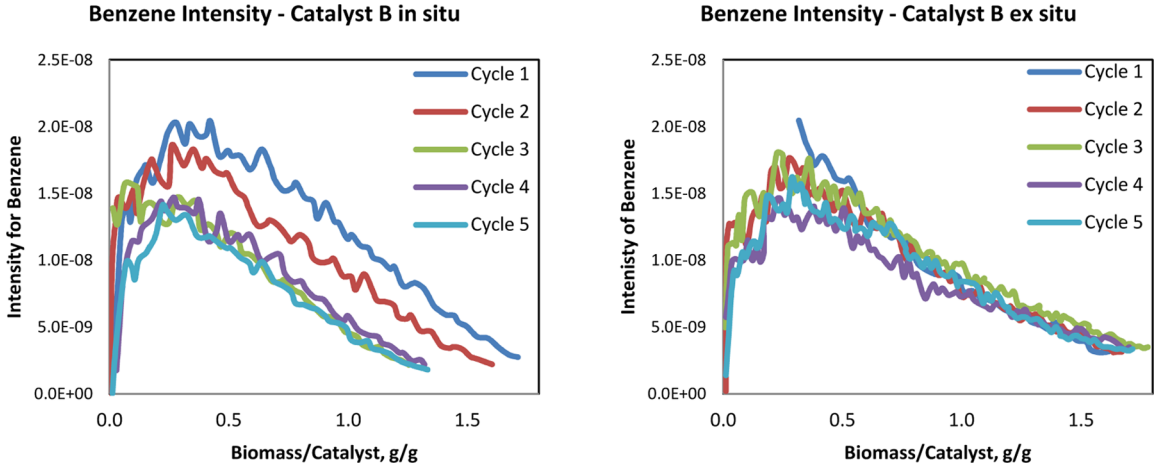

Figure 3. Benzene signal intensities (m/z = 78) during cycles 1−5 for in situ and ex situ catalytic pyrolysis with catalyst B.

3. RESULTS

3.1. Catalytic Cycles. Five catalytic cycles were completed in each series of experiments. Figure 2 compares the RGA signals for major hydrocarbons and oxygenates during one catalytic cycle as a function of the mass of biomass fed for both in situ and ex situ experiments. In general, similar profiles of hydrocarbons and oxygenates were obtained during all experiments. Toluene gave the highest signals in the experiments, followed by xylene. There was an initial increase in the hydrocarbon signals that can be attributed to the biomass feed rate being gradually increased in the beginning of the catalytic cycle. After the initial increase, the hydrocarbon signals decreased as the catalyst became deactivated.

Furan and phenol were the first oxygenates whose signals increased. These compounds are intermediates,[58] and often a maximum in their signal was identified. The signal for m/z 60, which could have been acetic acid or hydroxyacetaldehyde (labeled in the figure as acetic acid), started showing an appreciable increase only toward the end of the experiments. Other oxygenates whose signals became appreciable only toward the end of the runs and increased throughout the experiments were methoxyphenols. This is in accordance with the evolution

DOI: 10.1021/acs.energyfuels.5b02165
Energy Fuels XXXX, XXX, XXX−XXX

of products over HZM-5 while the catalyst deactivates, as determined in microscale experiments.[58]

Each catalytic cycle was continued as discussed above until the RGA indicated a significant drop in the signal for hydrocarbons and a rise in the signals for oxygenates. In particular, we followed the signals for toluene (m/z = 91) and acetic acid (m/z = 60). Figure 3 shows the variation in benzene signals between cycles during in situ and ex situ catalytic pyrolysis with catalyst B. For the ex situ experiment, no loss in benzene signal between cycles was observed. For the in situ experiment, the benzene levels decreased from cycle 1 to cycle 3 but appeared to remain constant in cycles 3−5. This suggests loss of the catalyst activity in the in situ configuration during the first cycles.

The ratios of biomass fed in each cycle to the catalytic mass for each cycle are summarized in Table 3. The amount of biomass fed in each cycle was based on the criterion of similar activity loss. As discussed above, the activity of the catalyst in the ex situ experiment with catalyst B remained relatively constant in each cycle; hence, there was little variation in the amount of biomass fed in each cycle. In the in situ experiment, in contrast, a loss in the catalyst activity was observed, and consequently, there is a decreasing trend in the amount of catalyst fed in each cycle. With catalyst A, significant reductions in the hydrocarbon mass signals were observed from one cycle to the next; consequently, the mass fed in each cycle was reduced significantly, as seen in Table 3. On the basis of this observation, catalyst B was selected for the in situ vs ex situ comparison. However, with catalyst A, all the signal intensities decreased for each cycle and were extremely low in the last two cycles, likely due to plugging of the capillary inlet to the RGA. It is thus possible that the loss in activity for this catalyst was not as significant as could be deduced from the decreases in the biomass-to-catalyst ratios.

Table 3. Biomass:Catalyst Ratio (biomass fed/catalyst, g/g) in Each Catalytic Cycle

cycle	catalyst A in situ	catalyst B in situ	catalyst B ex situ
1	1.72	1.71	1.52
2	1.35	1.61	1.72
3	1.05	1.47	1.78
4	1.01	1.32	1.70
5	0.71	1.34	1.72

3.2. Mass Balances. The overall mass balances for each experiment are shown in Table 4. Representative values for noncatalytic pyrolysis of pine in the same reactor system have been included in the table as reference. Due to the high water formation during catalytic pyrolysis, organic and aqueous liquids are separated, whereas only one liquid phase is formed in noncatalytic pyrolysis. There is not either any separate coke formation during noncatalytic pyrolysis. The total liquid yields were significantly reduced by catalytic pyrolysis and the gas yields increased. Relatively similar results were obtained in all the catalytic pyrolysis experiments: 37−42% of the input biomass was collected in liquids; the organic oil yield was 14−17% and the aqueous liquid yield 23−25%. The gas yields were 32−34% and the solid yields 16−18%. The coke yields were relatively constant at 7−9%. The liquid yields are in the same range as those reported in several other studies in fluidized bed reactor for woody biomass in both the in situ and ex situ configuration.[6,32,60]

Table 4. Total Mass Balance (g/g feed, %) on the Basis of Feed Pine

component		catalyst A in situ	catalyst B in situ	catalyst B ex situ	no catalyst[a]
liquids		40.6	41.9	37.2	66.9
	organic	17.3	16.9	14.1	
	aqueous	23.4	25.0	23.1	
gas		31.8	34.4	33.7	17.9
	light gases	25.8	28.1	28.4	17.9
	condensables	2.9	3.1	2.1	
	water	3.1	3.2	3.1	
solids		18.1	16.0	16.7	12.0
	char	9.6	8.8	8.8	12.0
	coke	8.5	7.2	7.9	
total		90.3	92.3	87.5	96.8

[a]Results for pine in Howe et al.[61]

The gas yields include condensable gases that were quantified from gas-bag samples taken during the catalytic cycles and water. These represent condensable materials that had escaped the condensation train. In less-dilute gas streams and with more efficient liquid capture, as would be likely in a larger scale system, a large fraction of the condensable gases could be captured as part of the liquids.

The mass balance closures were 88−92%. Mass balance closures measured in the same system for woody biomass in noncatalytic pyrolysis experiments are typically 92−97%.[61,62] Thus, there may have been loss of products not present in noncatalytic pyrolysis, such as coke or olefins or light organic components, whose formation is increased by catalytic pyrolysis. Volatile material losses during the catalytic cycles were estimated by the gas-bag samples, but there may have been additional losses during the catalyst regeneration, which took several hours in each cycle. The condensation train was sealed off during regeneration to prevent volatiles loss. However, any material that vaporized while the regeneration took place would have been lost when the gases were again switched through the condensation train.

3.3. Oil Analysis. Liquids were collected in three receivers in the condensation train. The first receiver from an air-cooled condenser contained a very viscous black liquid, the receiver from the ESP a slightly less viscous black liquid, and the receiver from the third condenser a yellowish aqueous liquid on top of which there was a thin layer of light-colored organic liquid. The liquid products were all combined and further separated in a separatory funnel. Three phases were obtained: top organic phase, middle aqueous phase, and bottom heavy organic phase. The bottom oil constituted the majority of the organic liquid: 88−89% of the organic phase for the experiments with catalyst B and >99% for the experiment with catalyst A. Each phase was analyzed separately with the exception of the top organic layer for the experiment with catalyst A, of which there was not a sufficient amount for analysis. The composition for the combined organic phase was then calculated on the basis of the analyses and masses of the phases. The yields and composition of the composite organic fraction and the aqueous fraction are in Table 5 and Table 6, respectively.

The analyses for the top and bottom oils are given in the Supporting Information. The top oils had lower organic oxygen contents than the bottom oils (7−8% vs 16−18%) and were also richer in hydrogen, as evidenced by the H:C molar ratio (1.15 vs 1.06−1.08). The top oils were also >95% volatile, as measured by proximate analysis (includes moisture and volatile matter measured at 750 °C).

The organic oxygen contents of the combined organic phases were 15.1−16.6%. Compared to the organic oxygen contents of

DOI: 10.1021/acs.energyfuels.5b02165
Energy Fuels XXXX, XXX, XXX−XXX

Table 5. Yields (%) and Composition of the Composite Organic Phase

	catalyst A in situ[a]	catalyst B in situ	catalyst B ex situ	no catalyst[c]
yield, g/g biomass	17.3	16.9	14.1	66.8
C yield, g C/g C in biomass	25.7	24.6	21.0	60.7
O yield, g O/g O in biomass	7.7	8.2	5.9	44.3
C, wt %	74.0	72.0	74.0	45.0
H, wt %	7.2	7.0	7.0	7.8
N, wt %	0.08	0.12	0.10	0.08
S, wt %	0.0	0.0	0.0	0.0
O, wt %	19.5	21.2	18.3	47.1
water (KF)	4.5	5.2	3.6	21.1
volatile matter, wt %	80.8	80.0	82.9	
fixed C, wt %	14.7	14.9	13.6	
ash, wt %	<0.05	<0.05	<0.05	
acid, mg KOH/g	4.2	4.8	3.0	39.6
organic O, wt %	15.5	16.6	15.1	28.3
organic H:C, mol/mol	1.08	1.08	1.07	
carbonyls, mol/kg[b]	1.51	1.71	1.60	

[a]Due to the small amount of the top phase for catalyst A, it was not analyzed. When calculating the composition of the combined organic phase, the composition of top organic phase was estimated as an average of those for catalyst B experiments. [b]Measured only in the bottom phase. [c]Results for pine in Howe et al.[61]

Table 6. Yields (%) and Composition of the Aqueous Phase

	catalyst A in situ	catalyst B in situ	catalyst B ex situ	no catalyst[a]
yield, g/g biomass	23.4	25.0	23.1	no separate aqueous phase
C yield, g C/g C in biomass	3.2	3.1	2.4	
O yield, g O/g O in biomass	45.5	49.4	46.2	
C, wt %	6.9	6.2	5.2	
H, wt %	10.5	10.6	10.6	
N, wt %	0.02	0.02	0.02	
S, wt %	<0.01	<0.01	<0.01	
O, wt %	82.5	83.7	84.7	
water (KF)	85.5	86.6	88.8	
volatile matter, wt %	14.5	13.4	11.2	
fixed C, wt %	<1	<1	<1	
ash, wt %	<0.05	<0.05	<0.05	
organic O, wt %	6.5	6.8	5.8	

noncatalytic pine pyrolysis oils prepared in the same reactor system (28%), this represents a reduction of ~45%.[61] The oxygen contents of the oils were comparable to those of other studies performed in fluidized bed reactors over ZSM-5 under similar conditions. For example, oil oxygen contents of 19% and 18% on dry oil basis have been reported for in situ and ex situ catalytic pyrolysis of woody biomass, respectively.[32,60] The slightly higher oxygen contents in those studies can be attributed to higher biomass-to-catalyst mass ratios than in our experiments (3 and 2.5 vs 1.5−1.7).

The acid contents of all organic phases were low, below a carboxylic acid number of 5. This is close to 90% reduction compared to noncatalytic pine pyrolysis oils prepared in the same reactor.[61] The carbonyl concentrations, which were measured only in the bottom fractions, were similar for all three experiments and less than half of typical values for raw pyrolysis oils.[57] The oil−water contents were also low (4−5%). Water is a significant product of upgrading of pyrolysis vapors over HZSM-5, but the product liquid separates into an aqueous and organic phase(s). Thus, the organic oils from catalytic pyrolysis oils have lower water contents than noncatalytic pyrolysis oils. The water content in the organic oils is dictated by the miscibility of water with the oil; thus, the oils with lower organic oxygen contents had lower water contents.

The total mass yields of the organic oil were in the range of 14−17% and were higher for the in situ than for the ex situ experiment. Similarly, the carbon yields were higher for the in situ experiments (24−25%). Even though the aqueous phase yields were high (23−25%), the carbon yields in the aqueous phase were relatively low: 2.4−3.2%. Thus, the aqueous phase does not represent a large loss of carbon. On the other hand, 46−49% of the oxygen in the feed was rejected as water.

The in situ configuration oil gave higher organic oil yield and also slightly higher oxygen and acid contents compared to the ex situ configuration. This suggests that the catalyst in the in situ experiment was more deactivated than the catalyst in the ex situ experiment. The in situ experiments also had a lower biomass-to-catalyst mass ratio (1.5 vs 1.8). Less biomass was passed over the catalyst in the in situ experiment, and this further suggests that the deactivation was faster than in the ex situ experiment. Yildiz et al.[48] reported both higher organic oil yield and higher aromatics contents (lower oxygen) in their in situ experiment compared to their ex situ one. This is in contradiction to our results. However, they used different reactors for the two configurations (auger and moving catalytic bed), which may have contributed to their result.

The organic and aqueous phases were analyzed by GC/MS. The compound classes are summarized in Figures 4 and 5. The organic phases consisted of aromatic hydrocarbons with a variety of oxygenates, similar to those measured in microscale experiments.[63,64] One- to two-ring aromatic compounds were predominant hydrocarbons in the top oils, whereas two-ring aromatics followed by three- and four-ring aromatics were the largest hydrocarbon group by area percentage in the bottom oils. The top oil oxygenates were dominated by phenols and furans. Naphthalenols, indenols, methoxyphenols, and phenols were the largest oxygenate groups in the bottom oils. In general, the bottom and top oils contained similar groups, but those present in the bottom oil were heavier. The compositions for the oils from the in situ and ex situ experiments with catalyst B were quite similar. The in situ oil had slightly more oxygenates, in accordance with the oxygen measurements.

The aqueous phase contained mainly light organics with cyclopenten-1-one being the dominant peak (30−60% of the total peak area measured). The aqueous phase from the experiments with catalyst A contained sugar fragments (10% of the area), while the in situ experiment with catalyst B showed evidence of trace levels of sugar fragments.

The NMR results are summarized in Figure 6. Aromatic C−C and C−H bonds dominated both organic fractions in all experiments. Aliphatic C−C were detected as well, and they likely consisted of side chains in the aromatic compounds, such as methyl groups in toluene, xylene, and methylnaphthalene. The largest oxygenate group was aromatic C−O; in addition, there were aliphatic C−O bonds (e.g., furans, ethers), methoxy groups (methoxyphenols), and C═O groups (aldehydes, ketones, and acids). These results agree with the GCSM measurements, which showed oxygenates with hydroxyl groups (phenols, methox-

DOI: 10.1021/acs.energyfuels.5b02165
Energy Fuels XXXX, XXX, XXX−XXX

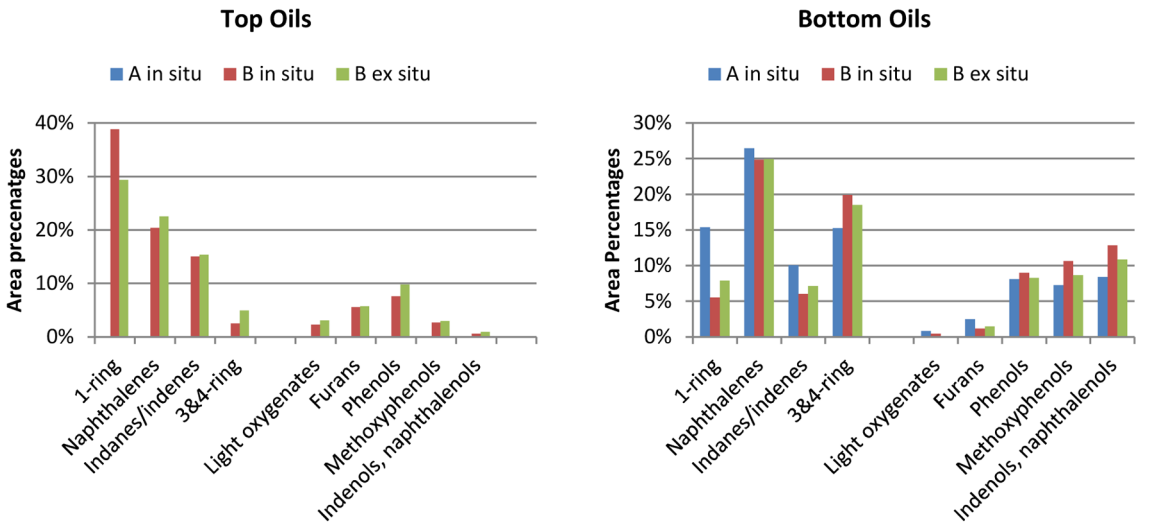

Figure 4. GC/MS analysis of the top and bottom organic fractions. The top oil for the experiment with catalyst A was not analyzed due to insufficient quantity.

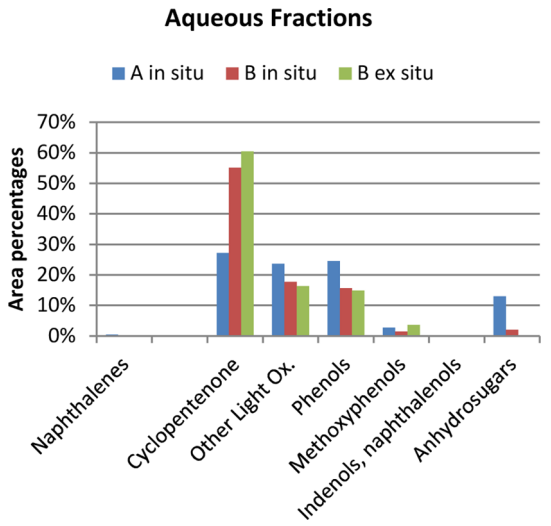

Figure 5. GC/MS analysis of the aqueous fraction.

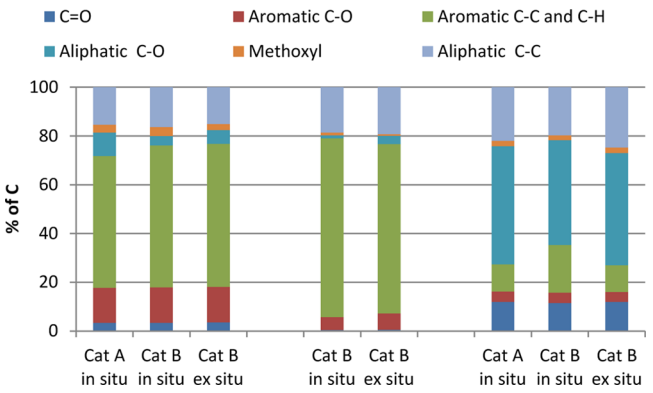

Figure 6. ^{13}C NMR analysis of the liquid fractions.

yphenols, indenols, naphthenols) as the dominant compounds with the presence of lower amounts of furans and light aldehydes and ketones. The top organic liquids had lower contents of carbon atoms with oxygen in them, in accordance with the lower O contents of these fractions. There were no significant differences between the in situ and ex situ oils. The oil from catalyst A had slightly higher aliphatic C−O contents compared to oils from catalyst B, which again confirms that the oil was more oxygenated and the catalyst more deactivated.

The aqueous fractions contained fewer aromatics than the organic fractions and were dominated by carbon atoms with oxygen attached to them. Aliphatic C−O groups were the largest group (~45% of all C), and the aqueous fractions also included more C═O groups compared to the organic fractions. Small amounts of phenolics were also present, as already suggested by the GC/MS analysis. The organics in the aqueous fractions consist of water-soluble molecules, mainly oxygenates of low molecular weights. These would include some light compounds, e.g. furan or light esters, which are covered by the solvent peak in the GC/MS analysis. This explains the higher aliphatic C−O content found in the aqueous phase by ^{13}C NMR than suggested by the GC/MS analysis. In contrast, the majority of the compounds in the organic fractions are heavier, and a good agreement between the NMR and GC/MS results is obtained.

The results from molecular weight distribution measurements are shown in Figure 7. In general, the molecular weight distributions were very similar for the three oils. The bottom oils show three peaks in the low molecular weight range and one broad peak in the high molecular weight range. The first three peaks correspond roughly to one-ring aromatics and oxygenates (e.g., benzene, 78; toluene, 92; xylene, 108; phenol, 94), two-ring aromatics and oxygenates (e.g., naphthalene, 128; methylindene, 134; methylnaphthalene, 142; dimethylnaphthalene, 156; naphthol, 146), and three- and four-ring aromatics (fluorene, 166; phenanthrene, 178; pyrene, 202; retene, 234). Compounds in this range were identified by GC/MS as well. Additionally, the molecular weight distribution showed a large, broad peak in the range of 250−3000. The top oils showed a preponderance of one-ring compounds with smaller peaks for two- and three-ring aromatics and even a small fraction of the high molecular weight compounds (peak at approximately 540). An analysis of the UV spectra suggested the presence of aromatics (for example naphthalene) and also phenolic compounds.

There was a good correspondence between the GC/MS analysis and the GPC results in the lower molecular weight range (one- to four-ring aromatics and oxygenates). However, the GPC

DOI: 10.1021/acs.energyfuels.5b02165
Energy Fuels XXXX, XXX, XXX−XXX

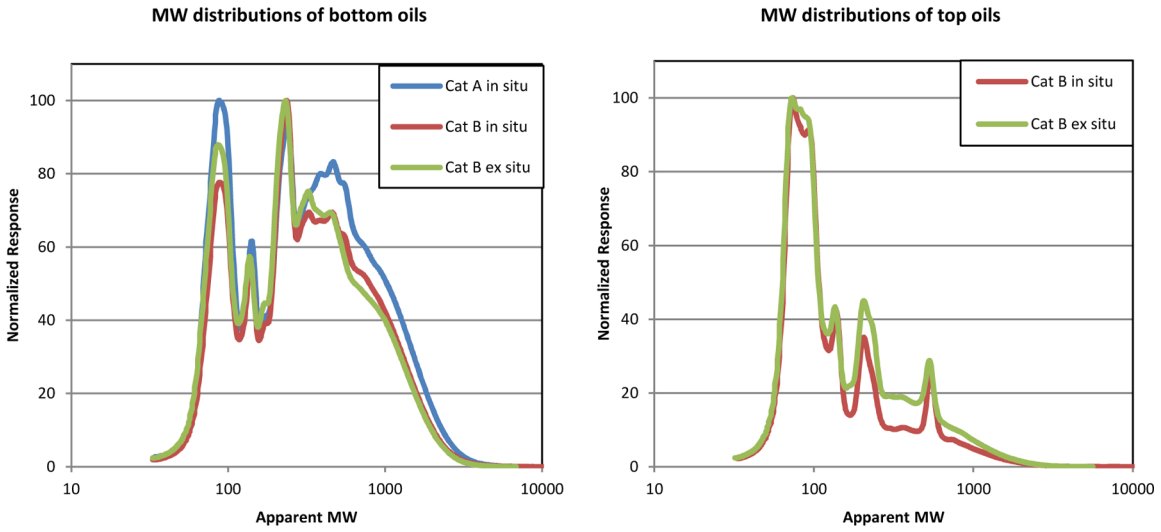

Figure 7. Molecular weight distributions measured for bottom and top oil fractions by GPC. Note the logarithmic scale of the *x*-axis.

revealed the presence of large fractions of high molecular weight material, which was not captured by the GC/MS.

The results of the aging test are depicted in Figure 8. The bottom oils were all of high viscosity initially, 3000−12000 mPa

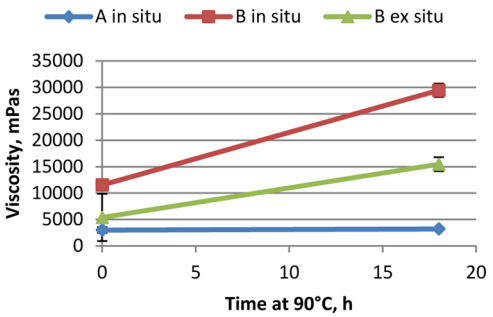

Figure 8. Results of the aging test of bottom oils.

s. The oil from the experiment with catalyst A showed no change in viscosity; thus, no aging was observed for this oil. The viscosities of the other oils changed by 150−190%, which was similar or slightly less than the change reported for noncatalytic pyrolysis oils from woody feedstocks.[65,66] It is not clear what caused the difference in the aging behavior between the oils. The oil from the experiment with catalyst A had overall the lowest biomass-to-catalyst ratio, lowest organic oxygen content, and lowest carbonyl content. Hence, it was the most upgraded oil and would be expected to have the least amount of aging reactions. However, the difference in the measured oil properties was not large and it is unclear whether this is sufficient to explain the difference. Further experiments with a wider variety of catalytic pyrolysis oils with different degrees of deoxygenation should be performed to verify the results.

3.4. Gas Analysis. The gases were analyzed for H_2, CO, CO_2, and C1−C4 hydrocarbons during the catalytic cycles by a micro-GC. A typical variation in the concentrations of the main gases during a catalytic cycle is shown in Figure 9. CO was present at the highest concentration, followed by CO_2. The slight increase in the signals in the beginning is due to ramping up of the biomass feed rate. CO_2, C_2H_4, and CO signals slightly decreased during the experiment, indicating a slight overall decrease in gas yield as the catalyst deactivated. CH_4 concentration slowly

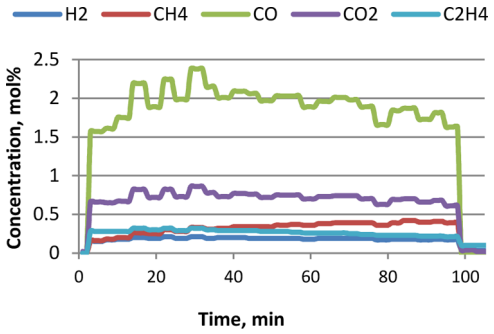

Figure 9. Variation of light gas compositions in cycle 4 for the ex situ experiment with catalyst B.

increased during the experiments. All experiments showed the same general trends, and there were no significant differences between the in situ and ex situ experiments.

Gas-bag samples were taken twice during most catalytic cycles, once in the beginning of the cycle and a second time toward the end of the cycle. The first sample represents the gas over an active catalyst and the second for a deactivated catalyst. The gases were analyzed by GC/MS-FID for light oxygenates and hydrocarbons. The results from the gas-bag analyses are summarized in Table 3 in the Supporting Information. The gases in the beginning of the experiments consisted mainly of hydrocarbons from benzene to naphthalene, and the gas bags taken from the end of the runs contained light oxygenates with small quantities of hydrocarbons. Acetaldehyde was the oxygenate with the highest concentration, followed by furan. Overall, the light condensables constituted 2−3% of the total feed and 3−4% of the carbon in the feed.

The yields of the individual gas compounds and the total mass, carbon, and oxygen yields are summarized in Table 7. H_2O was estimated as the saturation pressure at 0 °C, which was the measured temperature for the coalescing filter. The total gas yields were 32−34%, and the gas contained 27−29% of the feed carbon. Over 40% of the feed oxygen was rejected into gases. Compared to noncatalytic pyrolysis, the yield of CO was increased by a factor of 3, showing that decarbonylation is the predominant deoxygenation mechanism leading to carbon oxides during catalytic pyrolysis. The addition of catalyst also leads to increased formation of olefins, whereas formation of

DOI: 10.1021/acs.energyfuels.5b02165
Energy Fuels XXXX, XXX, XXX−XXX

Table 7. Yields (g/g feed, %) of Gas Compounds and Total Gas Yields

	catalyst A in situ	catalyst B in situ	catalyst B ex situ	no catalyst[a]
H_2	0.09	0.11	0.11	
CH_4	0.9	1.2	1.5	1.4
CO	14.2	15.7	15.8	5.4
CO_2	8.1	8.7	8.7	8.2
C_2–C_4	2.5	2.5	2.3	0.9
H_2O	3.1	3.2	3.1	
light condensables	2.9	3.1	2.1	
total yield, g/g feed	31.8	34.4	33.7	17.9
C yield, g C/g C in feed	26.7	29.0	27.8	11.9
O yield, g O/g O in feed	39.8	43.0	42.6	13.7

[a]Results for pine in Howe et al.[61]

CH_4 and CO_2 was similar to that for noncatalytic pyrolysis. No differences in the gas yields were observed between in situ and ex situ catalytic pyrolysis, suggesting that in situ and ex situ catalytic pyrolysis proceed via the same mechanism. In contrast, Wang et al.[51] reported higher olefin yields but lower aromatics yields from ex situ than in situ catalytic pyrolysis in the microscale. We observed lower aromatics yields for ex situ but not higher olefin yields. However, the study of Wang et al. was done at a significantly higher temperature of 700 °C, and their results indicated that the olefin yields for ex situ catalytic pyrolysis significantly increased as temperature was increased. Further, as discussed earlier, differences in the temperature profiles between in situ and ex situ modes in Py–GC/MS contribute to the differences observed in those types of experiments.

3.5. Solids Analysis. The solids formed consist of char, which refers to the material left from biomass after pyrolysis, and coke, which is formed on the catalyst from vapor-phase compounds. The measurements indicated some catalyst loss from the beds, 10% for catalyst A, 24% for catalyst B in the in situ configuration, and 10% for catalyst B in the ex situ configuration. The loss is attributed to entrainment of catalyst fines from the bed. The fines could have been present in the catalyst originally or formed via catalyst attrition. The higher loss of catalyst B in the in situ configuration could have contributed to the observed loss of catalytic activity between cycles.

The coke, char, and total solids yields are given in Table 8. There is some uncertainty in the separation between char and coke, but the error in yields is estimated to be less than one percentage point in both in situ and ex situ experiments. As described in the Experimental Section, the total solids formed and remaining in the system at the end of an experiment were determined by weighing; coke was calculated on the basis of the initial catalyst mass and catalyst solids analysis and char as the difference between the total solids formed and coke. In ex situ experiments, coke may be overestimated due to char blown into, and remaining in, the second reactor; in in situ experiments, the amount of coke may be overestimated by char remaining in the first reactor. On the basis of noncatalytic pyrolysis experiments performed in this reactor system, less than 5% of char remains in the first fluidized bed reactor or is collected later in the system. Each of these amounts correspond to less than 0.5 percentage points in yield. Together coke and char accounted for 16–18% of the mass and 25–26% of the carbon in the feed. Coke yields were 7–9% and coke accounted for 11–12% of feed carbon. A comparison of the in situ and ex situ experiments shows no difference in the amount of coke formed in the two configurations within the accuracy of the experiments. Yilditz et al.[48] had reported higher solid yields in ex situ than in in situ catalytic pyrolysis, but this was not supported in our study. As discussed earlier, in the study by Yildiz et al. the two reactors were not similar and this may have contributed to the differences in the solids yields.

Table 8. Coke, Char, and Total Solid Yields (%)

	catalyst A in situ	catalyst B in situ	catalyst B ex situ
	Coke		
yield, g/g feed	8.5	7.2	7.9
C yield, g C/g C in feed	11.8	11.1	12.2
O yield, g O/g O in feed	5.0	3.1	3.3
	Char		
yield, g/g feed	9.6	8.8	8.8
C yield, g C/g C in feed	14.3	13.9	13.9
O yield, g O/g O in fed	4.9	3.7	3.6
	Total Solids		
yield, g/g feed	18.1	16.0	16.7
C yield, g C/g C in feed	26.1	25.0	26.2
O yield, g C/g C in feed	9.9	6.8	6.9

A major mechanism of coke formation is via polymerization of aromatic compounds formed on the catalyst surface and in pores.[51] The oil yields for the two configurations were very similar, suggesting similar levels of aromatic coke precursors on the catalysts; consequently, coke formed via this mechanism would be expected to be similar in both configurations. Another mechanism suggested for coke is via deposition of lignin oligomers present in pyrolysis vapors. The concentration of the lignin oligomers could be expected to be different in the in situ experiments and ex situ experiments due to reactions taking place while pyrolysis vapors are transported from the first to the second reactor. The similar coke amounts in the two configurations suggest that coke formation from lignin derivatives is not significant.

The coke yields for the individual cycles are reported in Table 4 in the Supporting Information. In general, the coke yields were higher in the early cycles and decreased somewhat toward the later cycles. An exception was catalyst B in the in situ experiment, for which the coke yield was highest in the last cycle. It is possible that the coke had not become completely oxidized during the regenerations and more coke remained for the final measurements. Coke and char chemical analysis results are included in Table 3 of the Supporting Information. Both char and coke contained approximately 20% oxygen.

3.6. Catalyst Characterization. X-ray diffraction (XRD) was conducted on the fresh and spent ZSM-5 catalyst samples to examine their crystalline structure. The diffraction patterns for these materials are shown in Figure 10. The XRD profiles of the fresh and spent catalysts revealed the presence of the characteristic ZSM-5 crystalline structure. The spent materials all exhibit sharpened features near 27° and 46°, which we attribute to crystalline quartz species.

The acidity measurements are reported in Figure 11, and the corresponding NH_3 TPD profiles during these experiments are shown in Figure 12. Catalyst A had initially higher total acidity than catalyst B. The difference is likely a result of a combination of the amount of binder in the materials and the way in which the binder interacts with and/or blocks acid sites. However, the

DOI: 10.1021/acs.energyfuels.5b02165
Energy Fuels XXXX, XXX, XXX–XXX

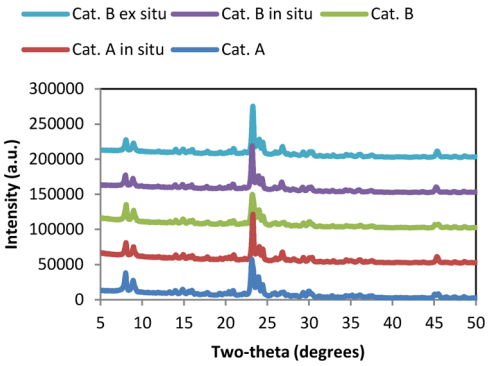

Figure 10. XRD patterns for fresh and spent catalysts.

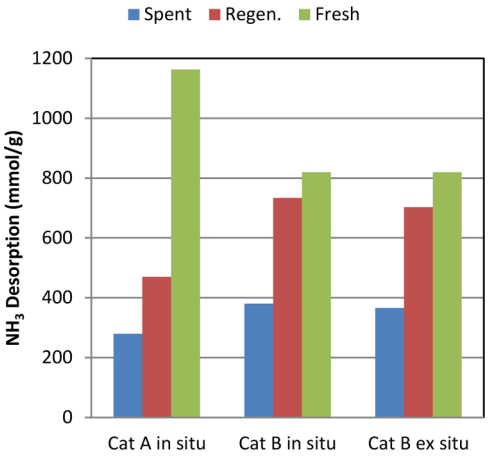

Figure 11. Acidity measurements from NH_3 TPD experiments for spent, regenerated, and corresponding fresh ZSM-5 samples. The masses of the spent catalysts were adjusted to eliminate contributions from coke deposits.

nature of the acid sites in terms of their desorption temperatures, which correspond to the sites' relative strengths, were similar for the two catalysts, as shown in Figure 12. Both exhibited two distinct desorption features, corresponding to weak acid sites (270 °C) and strong acid sites (450 °C).

Catalyst B showed essentially identical acidity at the end of the in situ and ex situ runs, and the extent to which they were regenerated was also nearly the same. The experiment with catalyst A led to a greater loss in acidity than either of the experiments with catalyst B, and the regeneration was also less complete. This is consistent with the online RGA results, which suggested a greater loss of activity during the catalytic cycles for catalyst A.

The NH_3 TPD profiles for the spent catalysts show that the strong acid sites are nearly completely absent for each sample. This suggests that during the course of the upgrading reaction, the strong acid sites are preferentially deactivated as compared to the weak acid sites. Following the regeneration, the NH_3 TPD profile shapes look quite similar to those of the fresh materials, indicating that both strong and weak acid sites were regenerated. For catalyst B from both experiments, the two types of sites are generally regenerated to the same extent, as the ratio of strong to weak acid sites (S/W) was nearly the same for the regenerated catalysts (0.43) and similar to that of the fresh material (0.41). Catalyst A had initially a higher S/W ratio of 0.54, which was reduced to 0.40 for the regenerated catalysts. Thus, strong acid sites appear to have been regenerated to a lesser extent than the weak acid sites for this catalyst. In contrast, Carlson et al.[43] reported loss of weak acid sites but not of strong acid sites after 10 reaction−regeneration cycles in a spouted bed in situ reactor. The degree to which strong and weak acid sites are regenerated may depend strongly on the catalyst and the binder.

The results for the activity measurements of the regenerated and coked catalysts performed in the analytical Py−GC/MS are summarized in Figure 13. Shown are the carbon yields (C in products divided by C in pine) in liquid-range hydrocarbon and oxygenated products. A more complete characterization of the products is given in the Supporting Information. For all the regenerated catalysts, hydrocarbons were the majority and 16−17% of the carbon was converted to these compounds. The hydrocarbons were mainly one-ring aromatics with smaller fractions of two-ring aromatics. Some oxygenates were present as well, and these were higher for catalyst B than for catalyst A. The oxygenates included acids (mainly acetic acid), ketones (e.g., butanone), and small amounts of furans and phenols.

For the coked catalysts, oxygenates were the major products with only minor amounts of hydrocarbons formed. The main oxygenate groups were carbonyls (e.g., hydroxyacetaldehyde), furans, methoxyphenols, phenols, and acids. The hydrocarbons were similar to the ones formed on regenerated catalysts, though a larger reduction was observed for one-ring hydrocarbons than for two-ring hydrocarbons. The results confirm those from the online RGA measurements, which showed that after regeneration the catalysts had high activity for hydrocarbon formation, but at the end of the cycles, the coked catalysts were indeed deactivated and produced little hydrocarbons. The deactivated catalysts gave overall higher carbon yields in liquid-range organic products than the regenerated catalysts but with higher oxygen contents.

The results from the activity measurements compared well with the RGA measurements during the runs. Both showed initially one-ring aromatics as the main products for the fresh catalyst. Very little hydrocarbons were formed in the end when the catalyst was coked. Both analyses showed furans, phenols, and acetic acid as important oxygenates. The oil GC/MS analysis suggested the products to be heavier than either the RGA or the catalyst activity tests suggested. Two-ring compounds were the aromatics with the highest peak areas in the oil analysis, whereas both the RGA and the activity tests showed more one-ring aromatics. It is possible that some of the light compounds were not properly captured in the condensation train or vaporized later. The contact pattern in the fluidized bed reactor may also increase the formation of heavier aromatics and explain why the oil was heavier than the activity measurements suggested. Longer contact times are expected to increase the fraction of heavier compounds. The gases also passed through a hot gas filter with a long residence time, and this could have contributed to molecular weight growth.

The catalyst activity tests also showed the coked catalyst from the in situ experiment to be more deactivated than that from the ex situ experiment (lower hydrocarbon yield and higher oxygenate yield), confirming the overall conclusion of faster deactivation in the in situ experiment. Py−GC/MS is thus a useful tool to compare activities of different catalysts. However, due to the different temperature profiles during in situ and ex situ configurations in these types of experiments, Py−GC/MS should not be used to compare the two configurations on a larger scale.

The NH_3 TPD measurements showed moderate decreases in the overall number of acid sites but large decreases in the number of strong acid sites. Per the activity measurements and the RGA

DOI: 10.1021/acs.energyfuels.5b02165
Energy Fuels XXXX, XXX, XXX−XXX

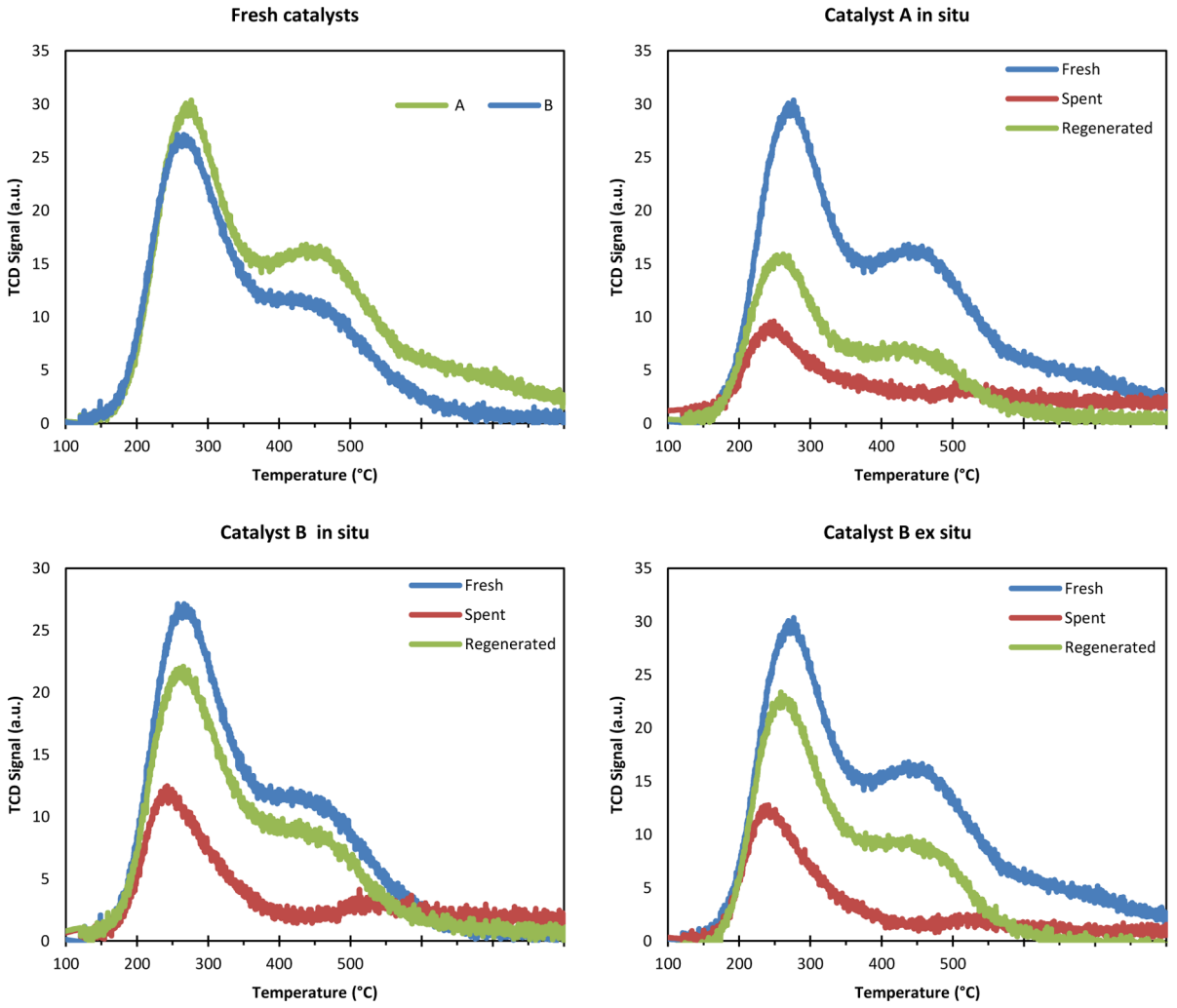

Figure 12. NH_3 TPD profiles for spent, regenerated, and the corresponding fresh ZSM-5 samples. At the end of the TPD, the catalysts were held at 500 °C for 30 min.

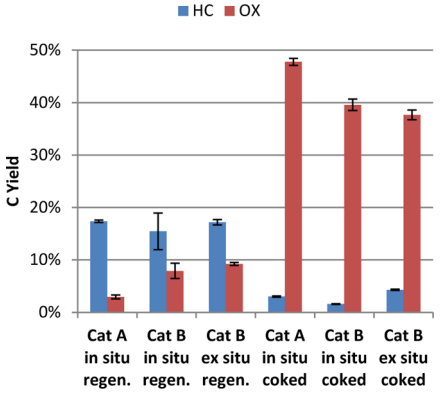

Figure 13. Carbon yields (g C in product/g C in biomass) in liquid-range hydrocarbon (HC) and oxygenate (OX) products for regenerated and coked catalysts measured in analytical Py–GC/MS. Pyrolysis temperature 500 °C, 10:1 catalyst:pine mass ratio.

data, the spent catalysts had lost the ability to upgrade pyrolysis vapors to hydrocarbons. This highlights the importance of strong acid sites in upgrading pyrolysis vapors.

The results of the ICP measurements for the fresh and regenerated catalysts are summarized in Figure 14. Fresh catalyst A had high contents of Ca, Fe, Na, and S, which are part of the clay binder. The contents of all of these elements were lower in the regenerated catalyst than in the fresh catalysts, which suggests loss of binder or binder components from the catalyst during the experiment. K, which was present at relatively high concentration in pine, had increased content in the regenerated catalyst from these experiments. Loss of some components, e.g., S, from both catalysts may be due to vaporization during time on stream or catalyst regeneration.

Catalyst B had a high Na content (approximately 0.24%) and its concentration remained relatively unchanged. The contents of several metals, notably K, increased during the experiments. K and Ca had increased concentrations for both in situ and ex situ experiments, whereas Fe and Mg had increased only for the in situ experiment. K, Ca, and Mg were the metals present at highest concentration in pine (Table 1), and the results indicate accumulation of them in the catalysts. Fe may originate from the reactor vessels or lines. The metals may bind to the acid sites and cause catalyst poisoning. Carlson et al.[43] similarly reported accumulation of K, Ca, Mg, and also Mn on catalysts from in situ catalytic pyrolysis in a spouted bed reactor.

These were short-term experiments—approximately 5 h total time on stream—and the accumulation of the metals may have contributed to the faster deactivation observed in the in situ experiment. At longer times typical of full-scale plants, the impact

DOI: 10.1021/acs.energyfuels.5b02165
Energy Fuels XXXX, XXX, XXX–XXX

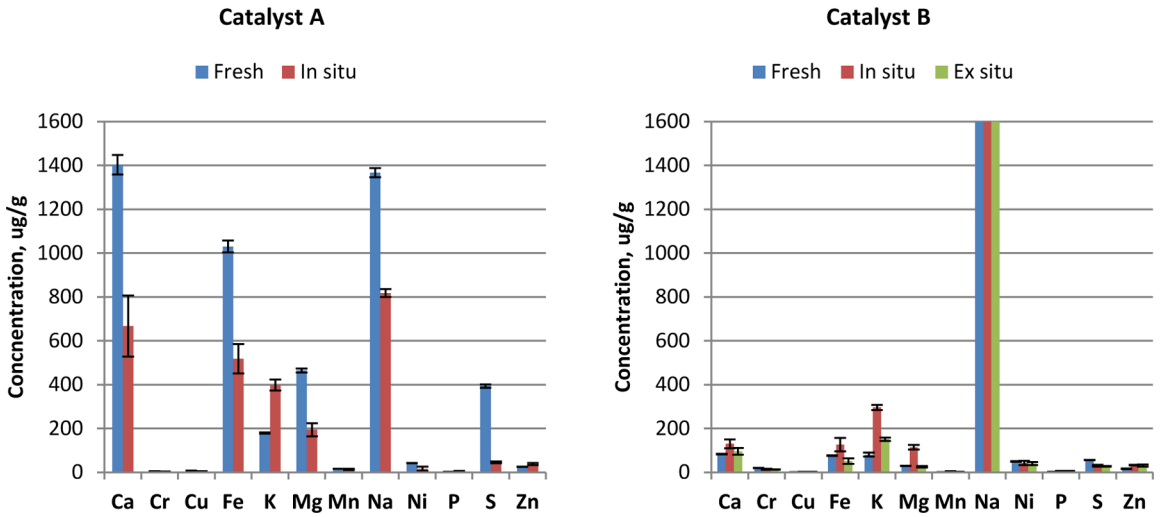

Figure 14. Contents of selected metals in fresh and regenerated catalysts.

of these contaminations may be significant. The problem with catalyst contamination is expected to be more serious for the in situ case, in which the catalyst is in direct contact with biomass and its ash constituents. Nevertheless, accumulation of some metals (K and some Ca and Zn) was evident in the ex situ experiment as well, though to a lesser extent than in the in situ experiment. The metals may enter the ex situ catalytic reactor either as fine particles (ash or char fragments) or as vapors. A hot-gas filter after the pyrolyzer has been found to be efficient in reducing the metal content in pyrolysis vapors[62,67] and could further mitigate the problem for ex situ catalytic pyrolysis.

4. CONCLUSIONS

Catalytic pyrolysis of pine vapors over HZSM-5 was studied in in situ and ex situ configuration in a bench-scale fluidized bed reactor system with two similar fluidized beds. The results indicated that the catalyst deactivated faster in the in situ configuration than the ex situ configuration, even in these short-term experiments. ICP analysis of the spent catalysts showed higher accumulation of metals from the in situ experiments, even after regeneration, which could be indicative of catalyst poisoning. No other significant differences between in situ and ex situ catalytic pyrolysis were observed, including in coke and gas yields or oil composition.

The oils had 65% lower oxygen contents than corresponding noncatalytic pyrolysis oils prepared in the same fluidized bed reactor system. High fractions of oxygen were rejected as water, CO, and CO_2, which indicates the importance of dehydration, decarbonylation, and decarboxylation reactions. Light gases were the main source of carbon losses, followed by char and coke. The loss of carbon in the aqueous phase was only about 3%.

Similar oil oxygen contents (15−17%), oil yields (14−17%), and carbon efficiencies (21−26%) could be obtained by both in situ and ex situ catalytic pyrolysis. The slightly better performance of in situ catalytic pyrolysis in terms of oil yield is offset by the higher propensity for catalyst deactivation. The total oil yields in both configurations are relatively low and present a substantial barrier for commercialization of the technology. Further development of both catalyst and process technology, with a focus on reducing losses to coke and light gases and improving yields of bio-oil intermediates, will be necessary to deliver economically competitive technology.

ASSOCIATED CONTENT

Supporting Information

The Supporting Information is available free of charge on the ACS Publications website at DOI: 10.1021/acs.energyfuels.5b02165.

Compounds for calibration of Py−GCMS, yields and composition of top and bottom organic phases, gases measured in gas-bag samples, and liquid-range hydrocarbons and oxygenates in Py−GCMS experiments with coked and regenerated catalysts (Tables 1−7) (PDF)

AUTHOR INFORMATION

Corresponding Author

*E-mail: kristiina.Iisa@nrel.gov.

Notes

The authors declare no competing financial interest.

ACKNOWLEDGMENTS

This work was supported by the U.S. Department of Energy under Contract No. DE-AC36-08GO28308 with the National Renewable Energy Laboratory. Funding provided by U.S. DOE Office of Energy Efficiency and Renewable Energy Bioenergy Technologies Office is gratefully acknowledged. We wish to thank Scott Palmer, Michele Myers, Ming Pan, Alexander Stanton, Matt Plumb, Bill Michener, Stuart Black, Steve Deutch, Renee Happs, Dr. Erica Gjersing, Dr. Calvin Mukarakate, and Dr. Robert Baldwin for their technical assistance and discussions.

REFERENCES

(1) Czernik, S.; Bridgwater, A. V. *Energy Fuels* **2004**, *18*, 590−598.
(2) Bridgwater, A. V. *Biomass Bioenergy* **2012**, *38*, 68−94.
(3) Sharma, R. K.; Bakhshi, N. N. *Can. J. Chem. Eng.* **1993**, *71*, 383−391.
(4) Adjaye, J. D.; Bakhshi, N. N. *Fuel Process. Technol.* **1995**, *45*, 161−183.
(5) Diebold, J.; Scahill, J. *ACS Symp. Ser.* **1988**, *376*, 31−40.
(6) Aho, A.; Kumar, N.; Eränen, K.; Salmi, T.; Hupa, M.; Murzin, D. Y. *Fuel* **2008**, *87*, 2493−2501.
(7) French, R.; Czernik, S. *Fuel Process. Technol.* **2010**, *91*, 25−32.
(8) Mihalcik, D. J.; Mullen, C. A.; Boateng, A. A. *J. Anal. Appl. Pyrolysis* **2011**, *92*, 224−232.
(9) Pattiya, A.; Titiloye, J. O.; Bridgwater, A. V. *J. Anal. Appl. Pyrolysis* **2008**, *81*, 72−79.

DOI: 10.1021/acs.energyfuels.5b02165
Energy Fuels XXXX, XXX, XXX−XXX

(10) Dutta, A.; Sahir, A.; Tan. E. ; Humbird, D.; Snowden-Swan, L. J.; Meyer, P.; Ross, J.; Sexton, D.; Yap, R.; Lukas, J. *Process Design and Economics for the Conversion of Lignocellulosic Biomass to Hydrocarbon Fuels. Thermochemical Research Pathways with In Situ and Ex Situ Upgrading of Fast Pyrolysis Vapors*; National Renewable Energy Laboratory: Golden, CO, 2015.
(11) Wan, S.; Wang, Y. *Front. Chem. Sci. Eng.* **2014**, *8*, 280−294.
(12) Diebold, J.; Scahill, J. *ACS Symp. Ser.* **1988**, *376*, 264−276.
(13) Horne, P. A.; Williams, P. T. In *Biomass for Energy and the Environment: Proceedings of the 9th European Bioenergy Conference*; Chartier, P., Ed.; Pergamon: Oxford, 1996; pp 1601−1606.
(14) Agblevor, F. A.; Rejai, B.; Evans, R. J.; Johnson, K. D. In *Energy from Biomass and Wastes XVI*; Klass, D. L., Ed.; Institute of Gas Technology: Chicago, 1992; pp 767−795.
(15) Williams, P. T.; Horne, P. A. *Fuel* **1995**, *74*, 1839−1851.
(16) Williams, P. T.; Horne, P. A. *J. Inst. Energy* **1996**, *69*, 176−191.
(17) Williams, P. T.; Nugranad, N. *Energy* **2000**, *25*, 493−513.
(18) Adjaye, J. D.; Bakhshi, N. N. *Fuel Process. Technol.* **1995**, *45*, 161−183.
(19) Vitolo, S.; Seggiani, M.; Frediani, P.; Ambrosini, G.; Politi, L. *Fuel* **1999**, *78*, 1147−1159.
(20) Cheng, Y.-T.; Jae, J.; Shi, J.; Fan, W.; Huber, G. W. *Angew. Chem., Int. Ed.* **2012**, *51*, 1387−1390.
(21) Karanjkar, P. U.; Coolman, R. J.; Huber, G. W.; Blatnik, M. T.; Almalkie, S.; de Bruyn Kops, S. M.; Mountziaris, T. J.; Conner, W. C. *AIChE J.* **2014**, *60*, 1320−1335.
(22) Agblevor, F. A.; Beis, S.; Mante, O.; Abdoulmoumine, N. *Ind. Eng. Chem. Res.* **2010**, *49*, 3533−3538.
(23) Agblevor, F. A.; Mante, O.; Abdoulmoumine, N.; McClung, R. *Energy Fuels* **2010**, *24*, 4087−4089.
(24) Mante, O. D.; Agblevor, F. A.; Oyama, S. T.; McClung, R. *Bioresour. Technol.* **2012**, *111*, 482−490.
(25) Mullen, C. A.; Boateng, A. A.; Mihalcik, D. J.; Goldberg, N. M. *Energy Fuels* **2011**, *25*, 5444−5451.
(26) Yang, H.; Coolman, R. J.; Karanjkar, P.; Wang, H.; Xu, Z.; Chen, H.; Moutziaris, T. J.; Huber, G. W. *Green Chem.* **2015**, *17*, 2912−2923.
(27) Zhang, H.; Xiao, R.; Huang, H.; Xiao, G. *Bioresour. Technol.* **2009**, *100*, 1428−1434.
(28) Zhang, H.; Xiao, R.; Wang, D.; Zhong, Z.; Song, M.; Pan, Q.; He, G. *Energy Fuels* **2009**, *23*, 6199−6206.
(29) Jae, J.; Coolman, R.; Mountziaris, T. J.; Huber, G. W. *Chem. Eng. Sci.* **2014**, *108*, 33−46.
(30) Aho, A.; Kumar, N.; Lashkul, A. V.; Eränen, K.; Ziolek, M.; Decyk, P.; Salmi, T.; Holmbom, B.; Hupa, M.; Murzin, D. Y. *Fuel* **2010**, *89*, 1992−2000.
(31) Aho, A.; Tokarev, A.; Backman, P.; Kumar, N.; Eränen, K.; Hupa, M.; Holmbom, B.; Salmi, T.; Murzin, D. Y. *Top. Catal.* **2011**, *54*, 941−948.
(32) Mante, O. D.; Agblevor, F. A. *Biomass Convers. Biorefin.* **2011**, *1*, 203−215.
(33) Mante, O. D.; Agblevor, F. A.; McClung, R. *Biomass Convers. Biorefin.* **2011**, *1*, 189−201.
(34) Atutxa, A.; Aguado, R.; Gayubo, A. G.; Olazar, M.; Bilbao, J. *Energy Fuels* **2005**, *19*, 765−774.
(35) Du, S.; Sun, Y.; Gamliel, D. P.; Valla, J. A.; Bollas, G. M. *Bioresour. Technol.* **2014**, *169*, 188−197.
(36) Stefanidis, S. D.; Kalogiannis, K. G.; Iliopoulou, E. F.; Lappas, A. A.; Pilavachi, P. A. *Bioresour. Technol.* **2011**, *102*, 8261−8267.
(37) Stephanidis, S.; Nitsos, C.; Kalogiannis, K.; Iliopoulou, E. F.; Lappas, A. A.; Triantafyllidis, K. S. *Catal. Today* **2011**, *167*, 37−45.
(38) Triantafyllidis, K. S.; Iliopoulou, E. F.; Antonakou, E. V.; Lappas, A. A.; Wang, H.; Pinnavaia, T. J. *Microporous Mesoporous Mater.* **2007**, *99*, 132−139.
(39) Iliopoulou, E. F.; Antonakou, E. V.; Karakoulia, S. A.; Vasalos, I. A.; Lappas, A. A.; Triantafyllidis, K. S. *Chem. Eng. J.* **2007**, *134*, 51−57.
(40) Iliopoulou, E. F.; Stefanidis, S.; Kalogiannis, K.; Psarras, A. C.; Delimitis, A.; Triantafyllidis, K. S.; Lappas, A. A. *Green Chem.* **2014**, *16*, 662−674.
(41) Lappas, A. A.; Samolada, M. C.; Iatridis, D. K.; Voutetakis, S. S.; Vasalos, I. A. *Fuel* **2002**, *81*, 2087−2095.
(42) Park, H. J.; Park, Y.-K.; Kim, J.-S.; Jeon, J.-K.; Yoo, K.-S.; Yim, J.-H.; Jung, J.; Sohn, J. M. *Stud. Surf. Sci. Catal.* **2006**, *159*, 553−556.
(43) Carlson, T. R.; Cheng, Y.-T.; Jae, J.; Huber, G. W. *Energy Environ. Sci.* **2011**, *4*, 145−161.
(44) Lu, Q.; Zhu, X. F.; Li, W. Z.; Zhang, Y.; Chen, D. Y. *Chin. Sci. Bull.* **2009**, *54*, 1941−1948.
(45) Pattiya, A.; Titiloye, J. O.; Bridgwater, A. V. *J. Anal. Appl. Pyrolysis* **2008**, *81*, 72−79.
(46) Torri, C.; Reinikainen, M.; Lindfors, C.; Fabbri, D.; Oasmaa, A.; Kuoppala, E. *J. Anal. Appl. Pyrolysis* **2010**, *88*, 7−13.
(47) Zhu, X.; Lu, Q.; Li, W.; Zhang, D. *Front. Energy Power Eng. China* **2010**, *4*, 424−429.
(48) Yildiz, G.; Pronk, M.; Djokic, M.; van Geem, K. M.; Ronsse, F.; van Duren, R.; Prins, W. *J. Anal. Appl. Pyrolysis* **2013**, *103*, 343−351.
(49) Gungor, A.; Onenc, S.; Ucar, S.; Yanik, J. *J. Anal. Appl. Pyrolysis* **2012**, *97*, 39−48.
(50) Nguyen, T. S.; Zabeti, M.; Lefferts, L.; Brem, G.; Seshan, K. *Biomass Bioenergy* **2013**, *48*, 100−110.
(51) Wang, K.; Johnston, P. A.; Brown, R. C. *Bioresour. Technol.* **2014**, *173*, 124−131.
(52) Gamliel, D. P.; Du, S.; Bollas, G. M.; Valla, J. A. *Bioresour. Technol.* **2015**, *191*, 187−196.
(53) Aho, A.; Kumar, N.; Salmi, T.; Holmbom, B.; Backman, P.; Hupa, M.; Yu Murzin, D.; Eranen, K. *Biofuels* **2010**, *1*, 261−273.
(54) Engtrakul, C.; Mukarakate, C.;, Starace, A. K.; Magrini, K. A.; Rogers, A. K., Yung, M. M. *Catal. Today* (in press) DOI: 10.1016/j.cattod.2015.10.032.
(55) Mukarakate, K.; Watson, M. J.; ten Dam, J.; Baucherel, X.; Budhi, S.; Yung, M. M.; Ben, H.; Iisa, K.; Baldwin, R. M.; Nimlos, M. R. *Green Chem.* **2014**, *16*, 4891−4905.
(56) Yung, M. M.; Stanton, A. R.; Iisa, K.; French, R. J.; Orton, K. A.; Magrini, K. A. Manuscript submitted to *Energy Fuels*.
(57) Nicolaides, G. M. Ph.D. Thesis, University of Waterloo, 1984, pp 17−26, 30−42.
(58) Ben, H.; Ragauskas, A. J. NMR Characterization of pyrolysis oils from kraft lignin. *Energy Fuels* **2011**, *25*, 2322−2332.
(59) Hill, H. H.; McMinn, D. G. *Chem. Anal. (Hoboken, NJ, U. S.)* **1992**, *121*, 15−21.
(60) Mante, O. D.; Agblevor, F. A. *Green Chem.* **2014**, *16*, 3364−3377.
(61) Howe, D.; Santosa, D.; Kutnyakova, I.; Lukins, C.; Westover, T.; Emerson, R.; Carpenter, D.; Deutch, S.; Starace, A. *Energy Fuels* **2015**, *29*, 3188−3197.
(62) Elliott, D. C.; Wang, H.; French, R.; Deutch, S.; Iisa, K. *Energy Fuels* **2014**, *28*, 5909−5917.
(63) Elliott, D. C.; Oasmaa, A.; Preto, F.; Meier, D.; Bridgwater, A. V. *Energy Fuels* **2012**, *26*, 3769−3776.
(64) Mukarakate, C.; Zhang, X.; Stanton, A. R.; Robichaud, D. J.; Ciesielski, P. N.; Malhotra, K.; Donohoe, B. S.; Gjersing, E.; Evans, R. J.; Heroux, D. S.; Richards, R.; Iisa, K.; Nimlos, M. R. *Green Chem.* **2014**, *16*, 1444−1461.
(65) Diebold, J. P.; Czernik, S. *Energy Fuels* **1997**, *11*, 1081−1091.
(66) Oasmaa, A.; Kuoppala, E. *Energy Fuels* **2003**, *17*, 1075−1084.
(67) Baldwin, R. M.; Feik, C. J. *Energy Fuels* **2013**, *27*, 3224−3238.

DOI: 10.1021/acs.energyfuels.5b02165
Energy Fuels XXXX, XXX, XXX−XXX

Supporting Information

Table 1. Compounds for calibration of Py-GCMS

Benzene	Acetaldehyde	Phenol
Toluene	3-Buten-2-one	Phenol, 2-methyl-
Ethylbenzene	2-Cyclopenten-1-one	Phenol, 3-methyl-
p-xylene	2-Cyclopenten-1-one, 2-methyl-	Phenol, 4-methyl-
o-xylene	2-hydroxy-3methyl-2-cyclopentenone	Phenol, 2,3-dimethyl-
Benzene, 1,2,3-trimethyl-	Furan	Phenol, 2,4-dimethyl-
Indane	Furan, 2-methyl-	Phenol, 2,3,5-trimethyl
Indene	Furan, 2,5-dimethyl-	1,2-Benzenediol
Naphthalene	Furfural	1,2-Benzenediol, 4-methyl-
Naphthalene, 1-methyl-	Benzofuran	Phenol, 2-methoxy-
Naphthalene, 2-methyl-	Benzofuran, 2-methyl-	Phenol, 2-methoxy-4-methyl-
Naphthalene, 1,6-dimethyl-	1-Naphthalenol	Phenol, 4-ethyl-2-methoxy-
Phenanthrene	Vanillin	2-Methoxy-4-vinylphenol
		Phenol, 2-methoxy-4-(1-propenyl)-

Table 2. Yields and composition of top organic phase

Experiment	Catalyst A in situ*	Catalyst B situ	Catalyst B ex situ
Yield, g/g biomass	0.04%	2.06%	1.54%
C Yield, g C/g C in biomass	NA	4.1%	3.1%
O Yield, g O/g O in biomass	NA	0.33%	0.29%
C, wt %	NA	85.6%	84.3%
H, wt%	NA	8.3%	8.1%
N, wt%	NA	0.03%	0.04%
S, wt%	NA	0.01%	0.01%
O, wt%	NA	7.0%	8.3%
Water (KF)	NA	0.5%	0.7%
Volatile Matter, wt%	NA	97.6%	96.6%
Fixed C, wt%	NA	1.9%	2.7%
Ash, wt%	NA	<0.05%	<0.05%
Acid, mg KOH/g	NA	3.5	5.7
Organic O, wt%	NA	6.6%	7.6%
Organic H:C, mol/mol	NA	1.15	1.15

*Insufficient top organic sample for analysis. Composition assumed to be average of the other two experiments when calculating the composition of the combined organic sample.

Table 3. Yields and composition of bottom organic phase

Experiment	Catalyst A in situ	Catalyst B situ	Catalyst B ex situ
Yield, g/g biomass	17.2%	14.9%	12.5%
C Yield, g C/g C in biomass	25.7%	21.0%	18.3%
O Yield, g O/g O in biomass	7.7%	7.9%	5.6%
C, wt %	73.9%	70.1%	72.7%
H, wt%	7.2%	6.9%	6.9%
N, wt%	0.08%	0.13%	0.11%
S, wt%	0.0%	0.0%	0.0%
O, wt%	19.5%	23.2%	19.5%
Water (KF)	4.5%	5.8%	3.9%
Volatile Matter, wt%	80.8%	77.6%	81.2%
Fixed C, wt%	14.7%	16.7%	14.9%
Ash, wt%	<0.05%	<0.05%	<0.05%
Acid, mg KOH/g	4.2	5.0	2.7
Organic O, wt%	15.5%	18.0%	16.1%
Organic H:C, mol/mol	1.08	1.06	1.06
Carbonyls, mol/kg	1.51	1.71	1.60

Table 4. Gases measured by GCMS-FID in gas-bag samples. Given are the boiling point for the compound (bp) and the lowest (min), highest (max), and average concentration of the vapors.

	bp	Concentration, ppm		
Catalyst A in situ	°C	min	max	average
Acetaldehyde/	20			
1-Propene, 2-methyl-	-7	476	1383	820
Furan	31	209	514	300
1-Butene, 2-methyl-	39	0	32	18
1,3-Cyclopentadiene	41	0	57	27
Cyclopentene	44	0	31	8
2-Propenal, 2-methyl-	69	0	16	4
3-Buten-2-one	81	0	48	16
Furan, 2-methyl-	64	35	110	55
2-Cyclopenten-1-one	150	0	18	4
Benzene	80	90	285	212
Toluene	110	129	292	207
Ethylbenzene	136	4	11	6
p-Xylene	138	36	66	48
p-Xylene	140	4	12	8
Benzene, 1,2,4-				
trimethyl-	176	0	4	1
Naphthalene	218	0	2	1

	bp,	Concentration, ppm		
Catalyst B in situ	°C	min	max	average
Acetaldehyde/	20			
1-Propene, 2-methyl-	-7	474	1524	965
Furan	31	180	531	366
2-Butene, 2-methyl-	39	0	43	23
1,3-Cyclopentadiene	41	24	61	45
Cyclopentene	44	0	8	2
3-Buten-2-one	81	0	51	28
Furan, 2-methyl-	64	30	127	75
Furan, 2-methyl-	64	0	23	12
1,3-Cyclohexadiene?	80	0	30	11
1,3-Cyclohexadiene?	80	0	15	7
Benzene	80	92	235	165
Toluene	110	103	215	161
Ethylbenzene	136	0	20	10
Benzene, 1,3-dimethyl-	138	0	67	29
p-Xylene	140	0	15	6
Benzene, 1,2,3-trimethyl-	176	0	4	1
Indane	176	0	3	1
Indene	182	0	4	1
Naphthalene	218	0	2	0

		Concentration, ppm		
Catalyst B ex situ	bp, °C	min	max	average
Acetaldehyde/	20			
1-Propene, 2-methyl-	-7	0	1505	728
Furan	31	0	468	258
1-Butene, 2-methyl-	39	0	22	15
1,3-Cyclopentadiene	41	0	94	34
3-Buten-2-one	81	0	36	14
Furan, 2-methyl-	64	0	85	47
Benzene	80	56	249	110
Toluene	110	64	208	96
p-Xylene	138	9	20	13

Table 5. Coke yields from individual cycles. Coke from cycles 1-4 was calculated from the carbon released as CO and CO_2 during oxidation (adjusted by the coke carbon content) and the coke for cycle 5 from the analysis of the coked catalyst after the experiment.

Coke yield g/g feed	**Catalyst A** **in situ**	**Catalyst B** **In situ**	**Catalyst B** **ex situ**
Cycle 1	9.2%	7.9%	9.4%
Cycle 2	9.1%	8.1%	9.9%
Cycle 3	10.1%	6.1%	8.3%
Cycle 4	8.1%	5.2%	7.3%
Cycle 5	6.4%	8.9%	6.3%

Table 6. Coke and char composition on ash and water-free basis.

Coke composition, **water-free basis**	**Catalyst A** **in situ**	**Catalyst B** **In situ**	**Catalyst B** **ex situ**
C, wt%	69%	77%	77%
H, wt%	5%	4%	4%
N, wt%	1%	1%	1%
O, wt%	25%	19%	18%
Char Composition, **Ash and water-free basis**	**Catalyst A** **in situ**	**Catalyst B** **In situ**	**Catalyst B** **ex situ**
C, wt%	73.6%	78.1%	78.5%
H, wt%	3.7%	3.6%	3.6%
N, wt%	0.2%	0.2%	0.2%
O, wt%	22.3%	18.1%	17.7%
S, wt%	0.1%	0.0%	0.0%

Table 7. Liquid-range hydrocarbons and oxygenates in py-GCMS experiments with coked and regenerated catalysts.

Temperature 500°C, catalyst:pine = 10.

	Cat A in situ regen'd	Cat B in situ regen'd	Cat B ex situ regen'd	Cat A in situ coked	Cat B in situ coked	Cat B ex situ coked
Hydrocarbons	**17.4%**	**15.4%**	**17.2%**	**3.0%**	**1.6%**	**4.3%**
Benzene	2.1%	1.7%	1.8%	0.0%	0.0%	0.0%
Toluene	4.4%	3.9%	3.9%	0.7%	0.3%	1.0%
Xylenes	5.2%	3.5%	5.0%	0.2%	0.2%	0.5%
Other 1-ring aromatics	1.3%	2.0%	2.0%	0.6%	0.5%	0.9%
Naphthalene	0.5%	0.5%	0.5%	0.0%	0.0%	0.1%
Alkylated Naphthalenes	2.1%	2.1%	2.4%	1.1%	0.1%	1.0%
Indanes/Indenes	1.2%	1.3%	1.2%	0.3%	0.3%	0.6%
Fluorenes	0.2%	0.3%	0.2%	0.1%	0.1%	0.1%
Phenanthrenes/ Anthracenes	0.4%	0.3%	0.3%	0.0%	0.1%	0.0%
Oxygenates	**2.9%**	**7.9%**	**9.2%**	**47.8%**	**39.6%**	**37.7%**
Acids	0.3%	3.1%	3.6%	4.9%	4.6%	4.7%
Aldehydes	0.1%	0.1%	0.1%	11.2%	9.3%	11.4%
Cyclopentenones	0.0%	0.2%	0.4%	1.8%	1.4%	1.7%
Other ketones	0.8%	1.3%	1.6%	7.6%	7.6%	8.0%
Furans	0.6%	0.7%	0.4%	11.5%	5.0%	2.1%
Indenols/Naphthols	0.2%	0.4%	0.7%	0.6%	1.5%	0.9%

Phenol	0.3%	0.3%	0.4%	0.3%	0.3%	0.3%
Alkylated Phenols	0.3%	0.7%	0.8%	3.2%	2.9%	2.9%
Catechols	0.0%	0.0%	0.1%	1.0%	1.4%	0.7%
Methoxyphenols	0.3%	0.8%	1.2%	4.8%	5.1%	4.6%
Methoxy Aromatics	0.0%	0.1%	0.1%	0.2%	0.3%	0.2%
Levoglucosan	0.0%	0.0%	0.0%	0.7%	0.1%	0.1%
Total	**20.3%**	**23.3%**	**26.4%**	**50.8%**	**41.2%**	**42.0%**